SCHOTTKY BARRIERS ON COMPOUND SEMICONDUCTORS:

I.   HgSe HIGHLY ELECTRONEGATIVE CONTACTS

II. Au SCHOTTKY BARRIERS ON $n\text{-Ga}_{1-x}\text{Al}_x\text{As}$

Thesis by

John S. Best

In Partial Fulfillment of the Requirements for

the Degree of

Doctor of Philosophy

California Institute of Technology

Pasadena, California

1979

(Submitted May 25, 1979)

To Dad and Mom

ACKNOWLEDGMENTS

I am deeply indebted to a great number of individuals who have helped to make my undergraduate and graduate stay at Caltech an enjoyable and tremendously profitable experience. I regret that I am only able to thank a few of them, who have contributed in a direct way to make this thesis possible.

I owe many thanks to J. O. McCaldin for his patient teaching and helpful advice. His encouragement, support, and equipment have made the work presented here possible. The many discussions we have had over both new and old ideas have provided many of the most enjoyable moments I have had over the past four years.

T. C. McGill and C. A. Mead have made immeasurable contributions to my education both through their classes, and through the many discussions that I have had with them. I have also learned a great deal from many hours of discussion with R. A. Scranton. The four men above have made the greatest direct impact upon my graduate career.

I would like to thank J. W. Mayer and M-A Nicolet for occasional use of their equipment, Thad Vreeland for use of his x-ray equipment, and S. S. Lau for help with both x-ray and backscatter measurements. I owe much to Lee Tutt for working out the CVD thermodynamics and performing the initial HgSe CVD growth experiments; and to P. C.

ABSTRACT

I.   HgSe is deposited on various semiconductors, forming a semimetal/semiconductor "Schottky barrier" structure. Polycrystalline, evaporated HgSe produces larger Schottky barrier heights on n-type semiconductors than does Au, the most electronegative of the elemental metals. The barrier heights are about 0.5 eV greater than those of Au on ionic semiconductors such as ZnS, and 0.1 to 0.2 eV greater for more covalently bonded semiconductors. A novel structure, which is both a lattice matched heterostructure and a Schottky barrier, is fabricated by epitaxial growth of HgSe on CdSe using hydrogen transport CVD. The Schottky barrier height for this structure is 0.73 ± 0.02 eV, as measured by the photoresponse method. This uncertainty is unusually small; and the magnitude is greater by about a quarter volt than is achievable with Au, in qualitative agreement with ionization potential arguments.

II.   The Schottky barrier height of Au on chemically etched n-$Ga_{1-x}Al_xAs$ was measured as a function of x. As x increases, the barrier height rises to a value of about 1.2 eV at $x \approx 0.45$, then decreases to about 1.0 eV as x approaches 0.83. The barrier height deviates in a linear way from the value predicted by the "common anion" rule as the AlAs mole fraction increases. This behavior is related to chemical reactivity of the $Ga_{1-x}Al_xAs$ surface.

Parts of this thesis have been previously presented in the following publications:

J. S. Best and J. O. McCaldin, "Lattice-Matched Heterostructures as Schottky Barriers: HgSe/CdSe", to be published, J. Vac. Sci. Technol.; also presented by J. S. Best at the Sixth Conference on the Physics of Compound Semiconductor Interfaces, Asilomar, California, February, 1979.

J. S. Best, "The Schottky Barrier Height of Au on n-Ga$_{1-x}$Al$_x$As as a Function of AlAs Content", Appl. Phys. Lett., $\underline{34}$, 522, 1979.

R. A. Scranton, J. S. Best, and J. O. McCaldin, "Highly Electronegative Contacts to Compound Semiconductors", J. Vac. Sci. Technol., $\underline{14}$, 930 (1977).

J. S. Best, J. O. McCaldin, T. C. McGill, C. A. Mead and J. B. Mooney, "HgSe, a Highly Electronegative Stable Metallic Contact for Semiconductor Devices", Appl. Phys. Lett., $\underline{29}$, 433 (1976).

Patent Application, "Mercury Chalcogenide Contact for Semiconductor Devices", application serial number 759,350; filed January 14, 1977. Inventors: James O. McCaldin and John S. Best.

TABLE OF CONTENTS

CHAPTER 1

FUNDAMENTALS AND MOTIVATION

A. INTRODUCTION

Metal-semiconductor interfaces have received a great deal of attention in recent years from both theoretical and experimental investigators, because of their importance in a wide variety of semiconductor devices. Rectifying metallic contacts, Schottky barriers, are vitally important in such circuits and devices as Schottky-clamped TTL, Schottky barrier gate field effect transistors (MESFETS), microwave diode mixers, and Schottky barrier solar cells. The work reported here deals with two areas in the field of Schottky barriers.

The first involves the use of a compound semimetal, HgSe, instead of an elemental metal to provide the Schottky barrier contact to a semiconductor. This contact provides extreme values for Schottky barrier heights, not obtainable with elemental metals, and can be fabricated as a lattice matched heterostructure with CdSe. These unique properties make the HgSe contact potentially useful for a number of devices and for developing a further understanding of Schottky barrier fundamentals. The second is the measurement of the Schottky barrier height of gold on $n\text{-}Ga_{1-x}Al_xAs$ as a function of x. These measurements were made to test the phenomenological rules of Schottky barrier heights across the alloy composition range of this technologically important compound semiconductor system.

B. BASIC REVIEW OF SCHOTTKY BARRIERS

As an introduction, let us begin with a basic review of Schottky barriers. A Schottky barrier is a metal-semiconductor junction, which typically has rectifying characteristics. Figure 1a shows the equilibrium band diagrams for typical Schottky barrier structures on n and p-type semiconductors. The Schottky barrier height, ϕ_n, for a metal on an n-type semiconductor is the energy barrier which an electron must surmount to go from the metal into the semiconductor. Thus, it is the energy difference, at the interface, between the semiconductor conduction band minimum and the Fermi level. Similarly, ϕ_p, on p-type semiconductors is the barrier for holes. Under forward bias, Fig. 1b, majority carriers can flow from the semiconductor to the metal over the reduced barrier, typically by the thermionic emission mechanism. Little current flows from the metal into the semiconductor under reverse bias; unless the barrier height is small, or the depletion layer is very thin.

Much of the recent work on Schottky barriers has concentrated on understanding what determines the Schottky barrier height for a given metal-semiconductor combination. A knowledge of the barrier height, and an ability to control it, is important for any techno-logically useful Schottky barrier. The barrier height is important in determining the current-voltage (both forward and reverse),
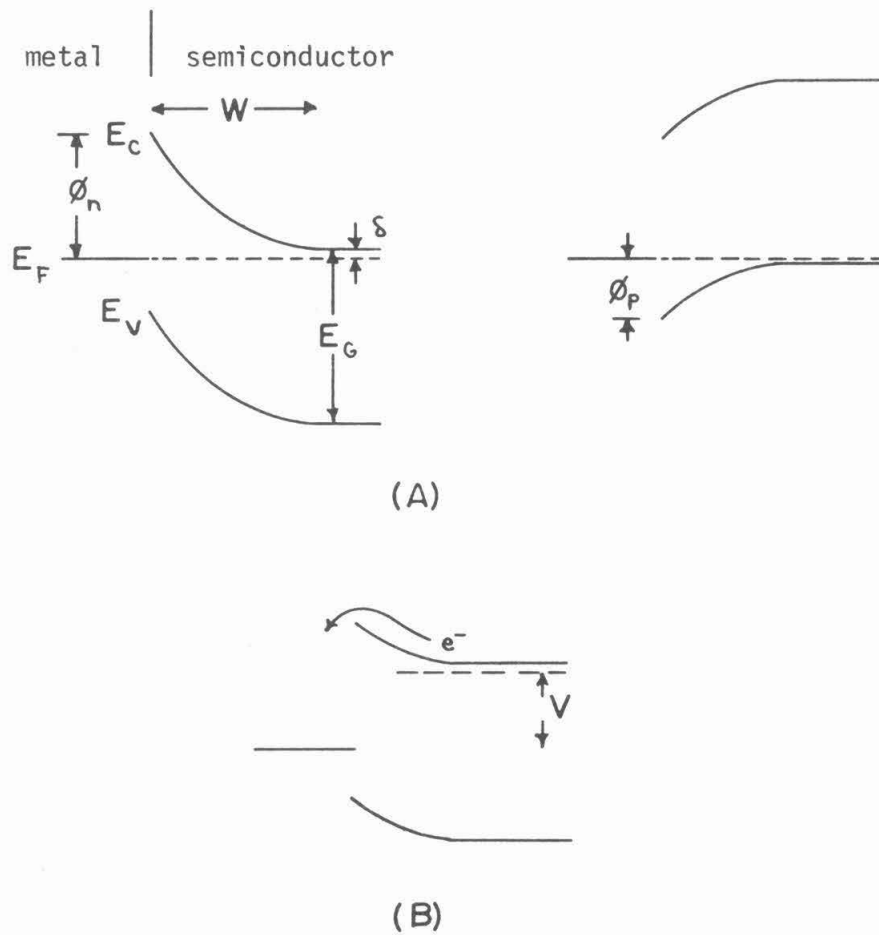
Fig. 1. (A) Equilibrium band diagrams for Schottky barriers on
n-type (left) and p-type (right) semiconductors. (B) Schottky on
an n-type semiconductor under forward bias. V is the forward bias
voltage.

capacitance-voltage, and other characteristics of the device. The
interfacial energies in a Schottky barrier are also closely related
to the characteristics of other semiconductor interfaces, such as
the semiconductor/vacuum interface, and the semiconductor/semiconductor
interface. All of these interfaces have found increasing use in
electronic devices. To cite only two critically important examples:
the MOS transistors used in the vast majority of LSI circuits today
depend on the semiconductor/insulator (usually Si/SiO_2) interface
for their basic operation; and semiconductor heterojunctions have
made low threshold, room-temperature continuous semiconductor lasers
possible.

C. SIMPLE MODELS AND PHENOMENOLOGY

The simplest and earliest method for predicting the Schottky
barrier height at a given metal/semiconductor interface is the Mott-
Schottky model [1]. Refer to Fig. 2 for a pictorial representation
of this model. The barrier height to n-type semiconductors is
found by assuming that the metal vacuum work function and the semi-
conductor electron affinity are fundamental quantities which do not
change as the metal/semiconductor interface is made. Taking the
vacuum level to be continuous, the difference in energy between the
semiconductor conduction band and the metal Fermi level, at the
interface, is equal to the difference between the semiconductor
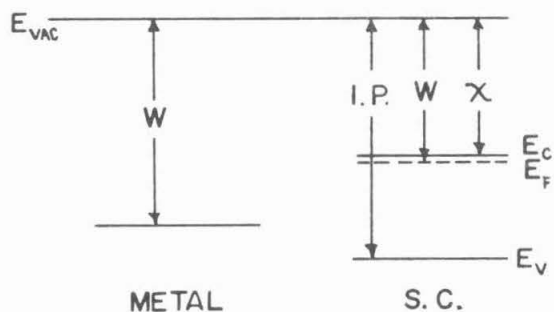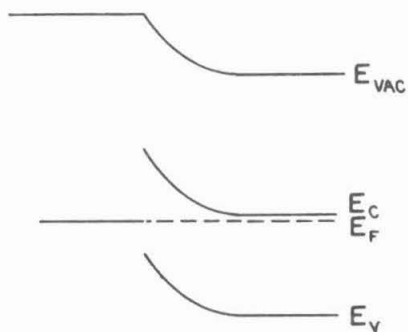
Fig. 2. Mott-Schottky model for predicting Schottky barrier heights. At (A), the energies of the metal and semiconductor bands with respect to vacuum before forming the Schottky barrier. At (B), the Schottky barrier is formed, with the energy relationships of (A) unchanged.

electron affinity and the metal work function.

This model assumes that any surface dipole contributions to
the metal work function and the semiconductor electron affinity are not
changed as the two materials are brought into intimate contact. It
also ignores the effect of any charged surface states in the semi-
conductor band gap. In practice, this model does not work well.
On the covalently bonded semiconductors, the Schottky barrier height
changes very little with metal work function [2], and on the ionic
semiconductors, the absolute values of the barrier heights are not
quantitatively correct. The sum of the barrier height to n-type and
p-type materials for a given metal-semiconductor combination does,
however, equal the band gap of the semiconductor, in most cases.
Hence, the energy of the Fermi level with respect to the band
edges, at the interface, does not change significantly as one con-
verts between p and n-type semiconductors.

Bardeen, in 1947 [3], proposed a model to explain the small
changes in barrier height on covalent materials with metal work func-
tion. He suggested that the Fermi level at the semiconductor surface
is pinned by the charging of surface states in the band gap of
the semiconductor. A separation of a very small distance - one inter-
atomic distance - between those surface states and the metal surface
can produce large voltage differences between the two. For example,

if a charge of 10^{14} electrons/cm^2, or one charge for every 10 surface atoms, is separated from the metal by only 1 Å, the voltage change across this interfacial dipole layer would be 1.8 volts (free space permittivity is assumed). A wide variety of theories have been proposed over the years to explain the cause and nature of the surface states. None of these has yet gained universal acceptance.

Since the development of these early models for Schottky barrier formation, many workers have amassed a great collection of empirical facts about Schottky barrier heights for different metal/semiconductor combinations. A set of empirical rules has developed from these facts. A few of those rules are detailed in the following paragraphs.

One of the earliest systematic observations was that the Schottky barrier heights of a given metal on the "p" and "n" types of the same semiconductor are simply related. The sum of ϕ_n and ϕ_p is equal to the semiconductor band gap. As stated earlier, this means that the Fermi level position, at the interface, with respect to the band edges of the semiconductor, is independent of the doping in the semiconductor. As an example, the barrier height of gold on n-GaAs is .90 eV and on p-GaAs is .42 eV [4]. $\phi_n + \phi_p = 1.32$ eV, fairly close to the band gap of 1.43 eV. It is important to note that this rule, like all of these empirical rules, is only approximate-

it can generally be trusted to within one or two tenths of a volt.
This is partly because of a large variability in the measured values
of Schottky barrier heights, and (probably) partly because these
rules are not themselves exact results of the fundamental physics of
Schottky barriers, but are approximate results, depending upon a
number of factors. Recent experimental results for Schottky barriers
fabricated in ultra-high vacuum on carefully cleaved surfaces indicate
that the $\phi_n + \phi_p = E_g$ rule may not always be true, even approximately.[5]

The second empirical rule is commonly known as the ionic-covalent
transition [2]. On the covalently bonded semiconductors, such as
Si, GaAs and InP, there is a very small change in barrier height with
different metals on the same semiconductor. $S \equiv \Delta\phi/\Delta\chi \approx 0$. Quantitatively,
the parameter S, defined as $\Delta\phi/\Delta\chi$, where χ is the metal Pauling electro-
negativity, is close to zero. For semiconductors with ionic bonding,
such as ZnS, there is a large change in the barrier height with metals
of different work function or electronegativity ($S\approx1$). For semiconduc-
tors with bonding between these two extremes, as determined by the dif-
ference in Pauling electronegativity between the cation and anion,
there is a sudden transition from one regime to the other. Although
many of the details of this transition are controversial, the essential
fact that barrier heights are almost independent of the metal on
covalent semiconductors and are strongly dependent on the metal for
ionic semiconductors is indisputable.

The final empirical rule that will be described here is illustrated in Fig. 3. Plotted in this figure, from McCaldin, McGill and Mead [7], are the conduction band edge, labeled by the semiconductor cation; and the valence band edge, labeled by the anion; with respect to the Fermi level for various gold/semiconductor interfaces. The difference in energy between the gold Fermi level and the semiconductor valence band at the interface, ϕ_p, in a gold/semiconductor Schottky barrier, is dependent only upon the anion of the semiconductor. For example, the barrier heights of gold on p-InP and p-GaP are both about 0.75 eV. In addition, this energy difference increases in a linear fashion with increasing electronegativity of the semiconductor anion.

This "common anion" rule is also valid for the semiconductor vacuum interface. The ionization potentials (electron affinity plus band gap) of most of the common III-V and II-VI semiconductors are dependent only on the anion, and increase in a linear fashion with increasing anion electronegativity. The slope of the linear relationship, however, is different than that for the Schottky barrier case.

Notice also that for most of the semiconductors in this diagram, the gold Fermi level at the interface is far from the valence band edge, even though gold is the most electronegative of the elemental metals. For the compounds with extremely low valence band energies,
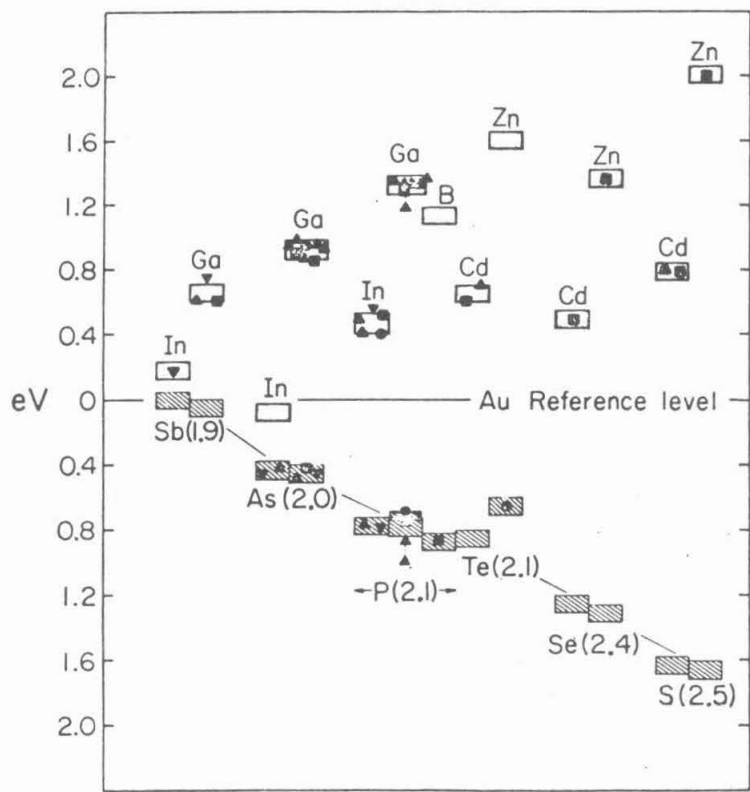
Fig. 3. Conduction band (labeled by semiconductor cation) and valence band (labeled by semiconductor anion) energies with respect to the gold Fermi level in gold/semiconductor Schottky barriers. The barrier to p-type semiconductors is dependent upon the anion only (from Ref. 7).

the selenides and sulfides, the Fermi level also cannot be brought close to the valence band in the bulk material; they cannot be doped significantly p-type. If a contact effectively more electronegative than gold is produced, it could move the Fermi level at the interface closer to the valence band than the elemental metals, providing higher barriers to n-type materials and lower barriers to p-type materials. Such a contact would be very useful for a variety of applications, such as light emitting diodes in ZnSe and ZnS, low leakage gates on InP MESFETS, Schottky barrier solar cells, or ohmic contacts to p-type materials. One such contact, polymeric sulfur nitride, $(SN)_x$, has been reported elsewhere [8]. The highly electro-negative properties of HgSe are described here.

Efforts to gain a fundamental understanding of the mechanism behind these empirical rules have not been completely successful as of the time of this writing.

Studies by various groups of cleaved semiconductor surfaces under ultra-high vacuum conditions have made some progress toward understanding the microscopic chemical and physical nature of the metal/semiconductor interface. Some of the key results will be briefly summarized here. Atomically clean, cleaved surfaces of III-V and II-VI compounds generally have no surface states within the forbidden gap of the semiconductor [9]. Thus, there is no band bending

in the semiconductor, and the Fermi level position with respect to the bands is the same at the surface as in the bulk. Submonolayer coverages of metals on the III-V compounds cause the formation of surface states which pin the Fermi level at the surface to the same position with respect to the bands as in a complete Schottky barrier [9]. This may be related to chemical and/or physical interactions between the metal and the semiconductor, which change the structure of the semiconductor surface and induce defects near the surface. Profiles of gold Schottky barriers on GaAs show either gallium or both gallium and arsenic throughout the gold layer, depending upon the method of surface preparation prior to the deposition [9,10]. Similar results have been obtained for GaSb and InP [9]. For further details on this work, the references should be consulted. As it relates to this thesis, the major conclusion of the fundamental Schottky barrier work to date has been that the metal/semiconductor interface, especially on the more covalently bonded compounds, is structurally very complicated. It is therefore extremely difficult to achieve a fundamental understanding of the observed Schottky barrier heights.

D. MERCURY CHALCOGENIDES

The common anion rule suggests that the mercury chalcogenide semimetals might act as more electronegative contacts than Au.

Figure 4 shows the common anion rule plot for the selenides only.
Starting with ZnSe, the gold barrier to n-type material is 1.36 eV,
placing the valence band energy 1.32 eV below the Fermi level.
Substituting Cd for Zn, the band gap shrinks from 2.67 to 1.74 eV.
The valence band position does not change; ϕ_n decreases by the same
amount as the band gap. If we extend the common anion rule to HgSe,
which has zero band gap, we would expect that the HgSe conduction
band minimum would lie significantly below the Au Fermi energy.
The question then becomes, if we use the HgSe as the metal in a
Schottky barrier to other semiconductors, will its valence band,
conduction band, and Fermi level lie lower in energy with respect to
the semiconductor's bands than does the Au Fermi level? If so, it
would produce higher barriers to n-type semiconductors and lower
barriers to p-type materials than Au.

An alternative way to view this question uses the common anion
rule for ionization potentials. A simple model for predicting band
discontinuities at semiconductor/semiconductor heterostructures is
to set the valence band discontinuity equal to the ionization potential
difference between the two semiconductors. This is equivalent to
the Mott-Schottky model for predicting Schottky barrier heights.
The difference is that, in this case, the model appears to work
fairly well. In GaAs/Ga$_{1-x}$Al$_x$As, only 15% of the band gap difference
appears in the valence band discontinuity [11]. This is in fairly
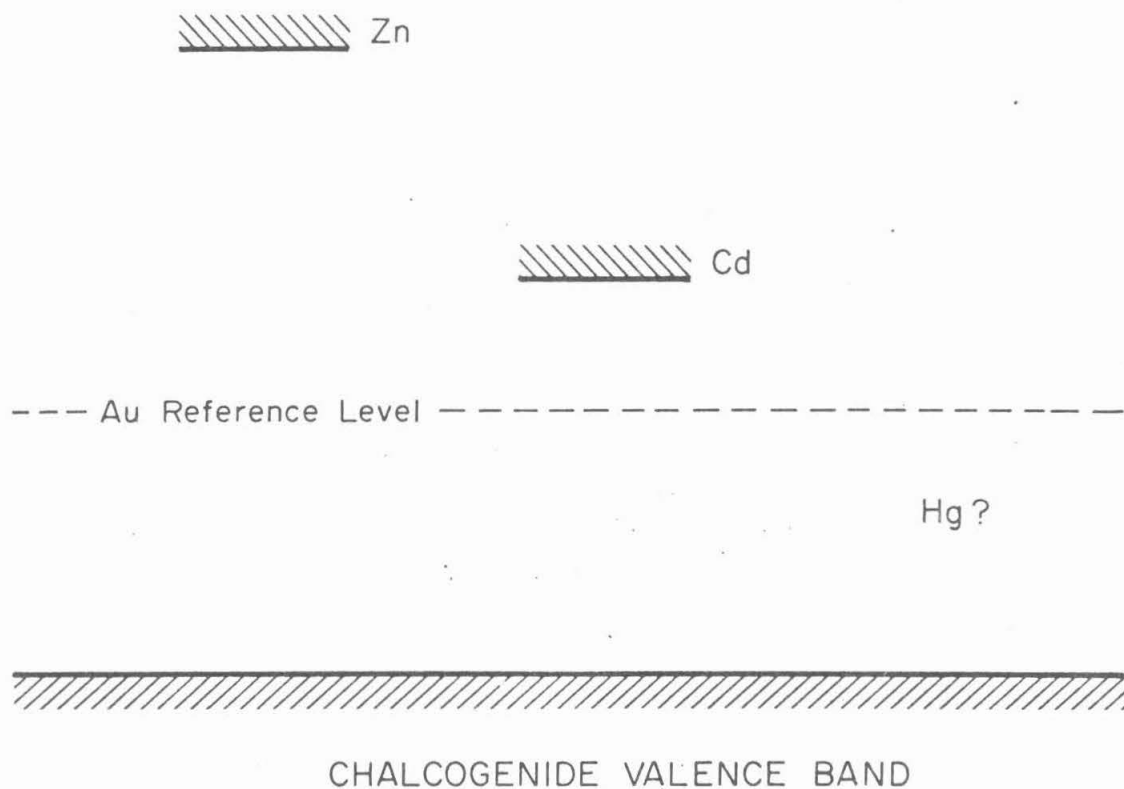
Fig. 4. A simplification of Fig. 3 for just the II-VI semiconductors. All of the tetrahedrally coordinated Hg chalcogenides are semimetals with zero band gap. This diagram suggests that the conduction band minimum of a Hg chalcogenide would lie below the Au reference level, thereby affording contact closer to the valence bands of common semiconductors. The positions shown are qualitative.

good agreement with the common anion rule prediction that it would be zero. Other combinations, such as InP/CdS [12] also follow this model approximately. For the case of HgSe/CdSe, the common-anion rule, combined with this simple heterostructure model, would predict that the valence bands would line up at the interface. Because the HgSe band gap is zero, this also means that the Fermi level at the interface would be close to the CdSe valence band. Therefore, the Schottky barrier height on n-CdSe would be close to the full band gap of the CdSe, 1.74 eV. The gold barrier height on n-CdSe is only 0.5 eV. Similarly, we would expect that the barrier height for HgSe on other n-type semiconductors would be larger than elemental metal barriers. These same arguments also apply to the other tetrahedrally coordinated mercury chalcogenides, HgTe and β-HgS. Because the electronegativity of sulfur is greater than that of selenium or tellurium, these simple ideas would predict that β-HgS would provide the largest difference with respect to Au of the three materials. HgTe would have a smaller difference.

Each of the mercury-chalcogenides has an interatomic spacing which is very close to that of the corresponding cadmium-chalcogenide (see Appendix I). This makes it possible to fabricate a device which is very similar to a Schottky barrier, yet is also a lattice-matched heterostructure. Such a structure has similar thermodynamic phases and bonding on either side of the interface, and is generally

much simpler in atomic structure than metal/semiconductor Schottky barriers. This provides an explanation for why the simple models are successful in predicting lattice matched heterostructure band lineups, but not in predicting metal/semiconductor Schottky barrier heights. The HgX/CdX heterostructure combines many of the features of Schottky barriers with the simplicity of a lattice matched heterostructure. There is, thus, a greater possibility of understanding the Schottky barrier heights from a more fundamental basis.

HgSe was chosen as the mercury-chalcogenide for initial experiments because it was likely to produce larger barriers on n-type materials than HgTe. The α, or cinnabar, phase of HgS is the equilibrium phase under standard conditions, so growth of a β-HgS contact was expected to be difficult. Epitaxial growth of HgSe on CdSe is also much easier to achieve than either HgTe on CdTe or β-HgS on CdS.

E.   Au on $Ga_{1-x}Al_xAs$

The common anion rule does not hold for all III-V and II-VI semiconductors. In Chapter 4, results of the measurements of gold on n-$Ga_{1-x}Al_xAs$, as a function of x, will be presented. Schottky barriers on GaAs, as shown in Fig. 2, fit the common anion rule very well. Barriers on AlAs do not. That chapter will discuss the failure as a function of the Al concentration in the alloy.

REFERENCES

1. E. H. Rhoderick, Metal-Semiconductor Contacts (Clarendon, Oxford, 1978), pp 20-24.

2. S. Kurtin, T. C. McGill, and C. A. Mead, Phys. Rev. Lett. 22, 1433 (1969).

3. op. cit., E. H. Rhoderick, pp 24-37.

4. C. A. Mead, Solid State Electron. 9, 1023 (1966).

5. W. E. Spicer, J. Lindau, P. W. Chye, P. Skeath, C. Y. Su, Sixth Annual Conference on the Physics of Compound Semiconductor Interfaces, Pacific Grove, CA, January, 1979.

6. L. Pauling, The Nature of the Chemical Bond (Cornell U., Ithaca, New York, 1960) 3rd ed., p 93.

7. J. O. McCaldin, T. C. McGill, and C. A. Mead, J. Vac. Sci. Technol. 13, 802 (1976).

8. R. A. Scranton, J. Appl. Phys. 48, 3838 (1977).

9. I. Lindau, P. W. Chye, C. M. Garner, P. Pianetta, W. E. Spicer, J. Vac. Sci. Technol. 15, 1332 (1978).

10. A. Hiraki, K. Shuto, S. Kim, W. Kammura, M. Iwami, Appl. Phys. Lett. 31, 611 (1977).

11. H. C. Casey, Jr., J. Appl. Phys. 49, 3684, (1978).

12. M. Bettini, K. J. Bachmann, E. Buehler, J. L. Shay, S. Wagner, J. Appl. Phys. 48, 1603 (1977).

CHAPTER 2

EVAPORATED HgSe

A. INTRODUCTION

In order to test the ideas of Chapter 1, two means of depositing HgSe on semiconductor substrates were developed. In this chapter, an evaporation scheme is discussed, which is useful for depositing HgSe thin films on any substrate. This method cannot easily be adapted to grow epitaxial single crystal HgSe, and hence was used only to test the barrier height of HgSe on various substrates. The lattice-matched Schottky, HgSe/CdSe, and an epitaxial technique for growing it, are discussed in Chapter 3.

Simple thermal evaporation has been used to deposit several of the II-VI compounds, notably ZnS and CdS [1,2]. Evaporation of HgSe has been reported in the literature [3], but deposited layers suffer from a severe deficiency of Hg. To achieve a stoichiometric deposition of HgSe, a means of reacting mercury with excess deposited selenium that is on the substrate must be used.

The first technique used by the author was to evaporate selenium dots onto the substrate, then react the selenium with mercury vapor. This was accomplished by placing the sample in a sealed evacuated tube along with a drop of mercury and heating to $100^{\circ}C$ for 15 minutes. The polycrystalline HgSe layers formed were very rough in texture and did not adhere well to the substrates (various III-V and II-VI semiconductors). The deposited amorphous selenium undergoes a phase transition to the equilibrium hexagonal phase

at roughly 70°C [4], and tends to ball up on the substrate in the
process. Then subsequent reaction with the mercury vapor again
changes the crystal structure and volume of the layer drastically.
The result was a poorly reproducible HgSe contact. Some electrical
measurements were made of HgSe on ZnS diodes made in this way. The
results were consistent with those obtained for improved HgSe films
to be described below.

An evaporative growth technique which avoids these problems is
molecular beam epitaxy (MBE) [5]. In MBE growth of GaAs, separate
molecular beams of gallium and arsenic impinge upon the substrate.
Arsenic will not stick to the substrate at the growth temperature
because of its high vapor pressure. Gallium does stick to the
substrate, and is delivered to the substrate at a rate of roughly a
monolayer per second. The arsenic flux is kept several times higher
than the gallium flux, so that as each monolayer of gallium condenses
on the growing GaAs surface, the arsenic reacts with the gallium to
form stoichiometric GaAs. Because the arsenic alone will not
stick, the arsenic flux is not critical. However, it must be large
enough compared with the gallium flux to insure complete reaction
of the gallium with arsenic before the next layer of gallium arrives
at the surface.

The same principle as used for GaAs MBE growth was applied to

HgSe. In this case, selenium has the lower vapor pressure, so it sticks to the room temperature substrate. A much higher flux of mercury then reacts with the selenium as it lands on the substrate.

B. HgSe EVAPORATOR

HgSe was deposited on samples using the apparatus shown in Fig. 1. This growth chamber, made of stainless steel and quartz, was placed inside a small vacuum system. The whole system was roughed with a vacsorb (liquid nitrogen cooled molecular sieve) roughing pump for about 10 minutes, then further evacuated to operating pressure with an ion pump. Liquid nitrogen filled cold fingers in the system aid the ion pump by providing a high pumping speed for water vapor desorbing from the chamber walls. The main vacuum chamber is about 10 cm in diameter and 10 cm high, allowing a short pumpdown time with a small ion pump. The inner growth chamber is about 5 cm in diameter and 2.5 cm high. The substrates were prepared as in Appendix II, and then cleaved in air and placed in the chamber immediately before pumpdown.

A drop of triple distilled mercury was placed inside the growth chamber on a quartz receptacle to provide Hg vapor for the growth. Hg pressure inside the chamber is determined by the mercury temperature (about $25^{o}C$), the relative areas of the hole in the base of the chamber
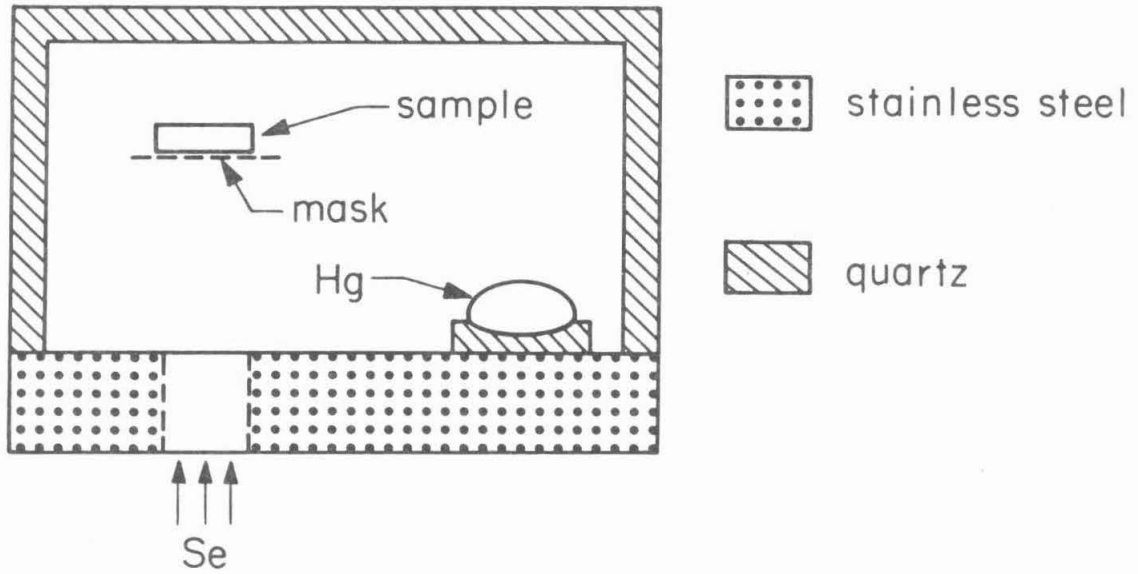
Figure 1. Schematic diagram of the HgSe growth chamber. The chamber is placed inside an ion-pumped vacuum system. Se is evaporated into the chamber from below, and, upon condensing onto the sample, reacts with Hg vapor present in the growth chamber to form HgSe.

and the mercury surface, and the cleanliness of the mercury surface. This establishes an Hg pressure of somewhat less than the room temperature vapor pressure of 1.4×10^{-3} Torr [6], so that mercury will not condense on either the specimen or the chamber walls. The cold fingers in the vacuum system effectively pump the mercury vapor which escapes from the inner chamber.

Selenium was evaporated at a rate of roughly one monolayer per second through a hole in the bottom of the HgSe growth chamber. The substrate was placed directly over the hole on a fine screen evaporation mask to define small (approximately 3×10^{-4} cm^2 area) dots of Se. Reaction between the evaporating selenium and mercury vapor present in the chamber takes place at room temperature to form stoichiometric HgSe as the selenium condenses. Pressure measured at the vacuum system ion pump was less than 10^{-6} Torr during the selenium evaporation.

Early experiments used a simple crucible evaporator as the selenium source, run at a temperature of about 200°C. On some samples, stoichiometric HgSe deposits were formed; on others, the deposit was reddish, indicating excess selenium. Without providing either very close control over the three parameters of selenium evaporation rate, substrate temperature, and Hg pressure in the growth chamber, or increasing the reaction rate of the condensing selenium with the Hg, consistent results could not be obtained.

Selenium vapor can exist as Se_2 or as ring structures with 3 to 8 atoms per molecule. At room temperature, the single bonded Se_5 and Se_6 ring structures are the most stable and are not very reactive [7]. Fig. 2, from data compiled by Berkowitz [8], shows the average number of Se atoms per molecule as a function of pressure, with temperature as a parameter. Vacuum system pressures are quite low; on this scale, they are essentially zero. Selenium has a very high evaporation rate at $250^{\circ}C$. If selenium is evaporated from an ordinary boat or shielded source, a large proportion of the selenium vapor consists of the stable ring structures. As the temperature of the vapor increases, the selenium rings apparently break into more reactive diatomic Se_2 molecules.

A selenium source was constructed to take advantage of the higher reactivity of the smaller selenium molecules. The selenium is heated in a boron nitride crucible to perhaps $250^{\circ}C$, which produces an adequate evaporation rate (see Fig. 3). The selenium vapor then passes through a hot quartz tube (roughly $700^{\circ}C$), where the Se_n ring structures in the vapor are cracked into smaller molecules. Two versions of the cracking tube were used. One consisted of a coiled tube with a length to diameter ratio of over 100 heated by a 13 mil diameter tungsten wire wrapped around the tube. The total length of the tube was about 200 mm. The other was a straight tube 40 mm long with a 2 mm i.d., heated in the same way. Both were apparently effective. Se_2 vapor coming out of the top of the tube was directed
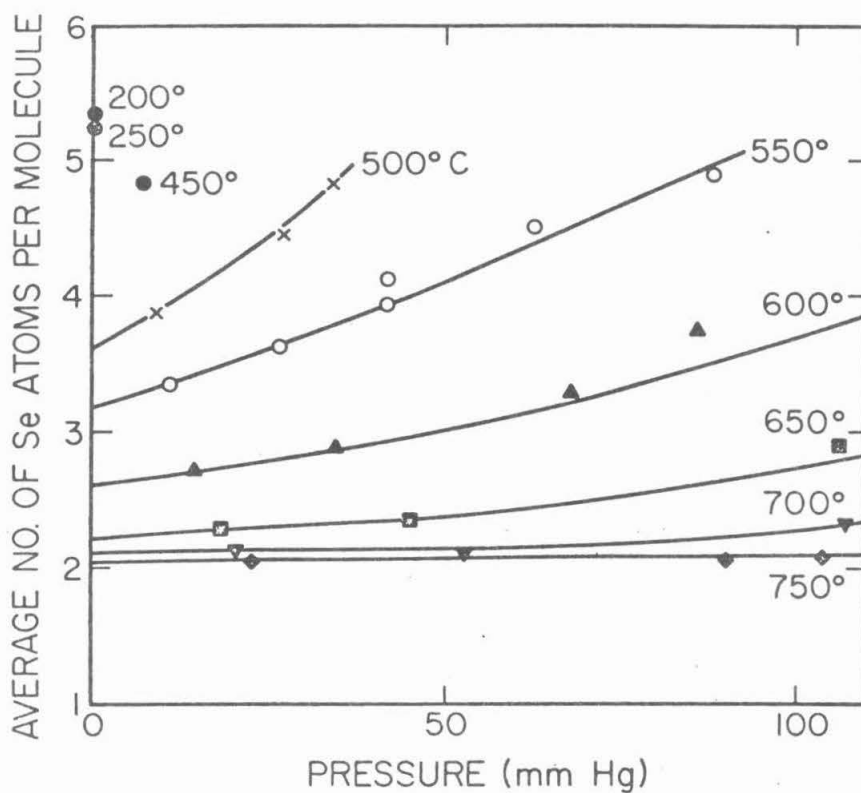
Figure 2. The average number of Se atoms in a molecule of Se vapor is plotted against pressure, with temperature as a parameter. Heating the Se vapor changes the stable ring structure molecules to the more reactive diatomic Se_2. (From data compiled by J. Berkowitz and W. A. Chupka, reference 8).
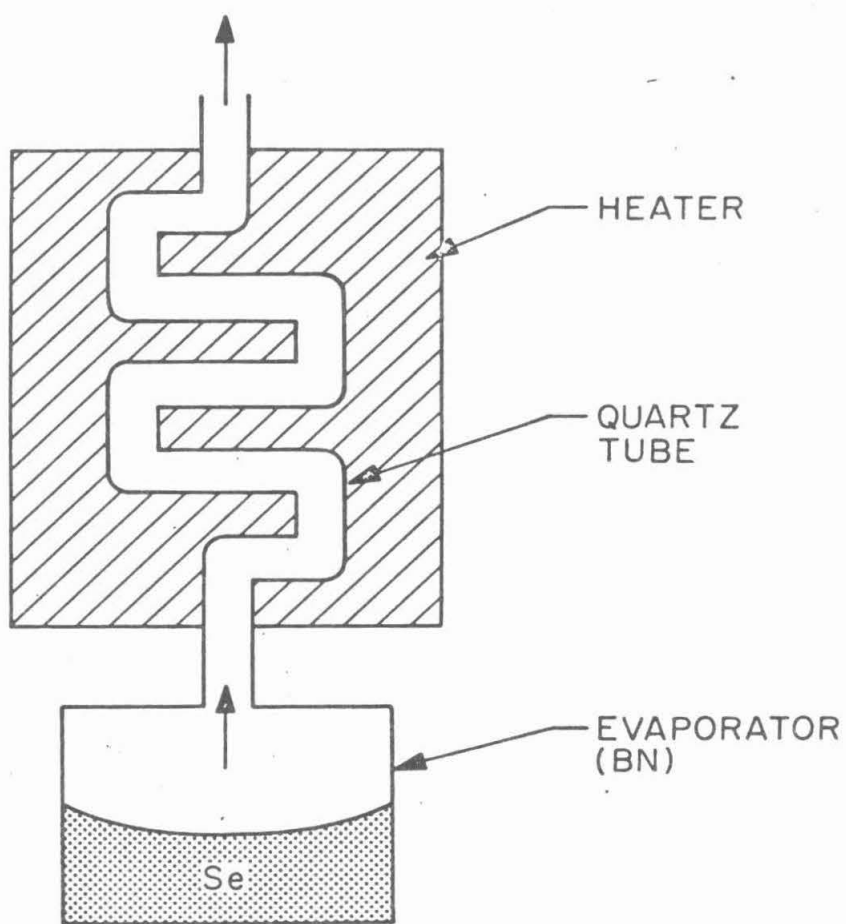
Figure 3. An apparatus to produce reactive Se_2 vapor. The temperature of the evaporator crucible determines the Se evaporation rate and the temperature of the coiled quartz tube adjusts the molecular weight of the Se vapor.

into the HgSe growth chamber shown previously. Use of this apparatus for the Se source resulted in consistent, stoichiometric HgSe deposition. Polycrystalline HgSe was also used for the selenium source material; it gave similar results, with a somewhat higher BN crucible temperature.

C. RESULTS

The HgSe surface appeared smooth under examination with a SEM, even at 20,000X magnification. Optically, the dots appeared to be shiny and black in color. As mentioned above, some of the samples using early selenium source designs showed dots with a reddish appearance. In extreme cases, this selenium rich film was not conductive.

Several of the samples which appeared to be good HgSe deposits, both optically and electrically, were examined with an electron microprobe. This showed the HgSe to be stoichiometric to within a few percent. One typical one week old HgSe on ZnS sample was examined by Auger electron spectroscopy to obtain a profile of the composition of the HgSe layer vs depth. No oxygen or carbon was detected in the HgSe layer and it was determined, to within the 10% accuracy of the method, that the layer is stoichiometric. The growth technique thus produced relatively pure HgSe that is stable in air. Some oxygen was found at the HgSe-ZnS interface.

Schottky barrier heights were measured using the current-voltage, capacitance-voltage, and photoresponse techniques. A brief description will be given here of each of these techniques; the reader is referred to the considerable literature on the subject for further information (9,10,11).

Forward current vs voltage of a Schottky barrier diode is most frequently determined by the thermionic emission mechanism. Under ideal thermionic emission, the forward current is given by $J = A(\frac{m^*}{m})T^2 e^{-\phi/kT}(e^{qV/kT}-1)$, where A is Richardson constant (120 A/cm^2), $(\frac{m^*}{m})$ is an effective mass correction to Richardson's constant, which takes into account the shape and orientation of the bands in the semiconductor, T is the temperature in ^oK, ϕ is the barrier height, and V is the forward voltage.

The barrier height can then be determined by plotting lnJ vs V as a straight line. The intercept at V=0 gives $\frac{-\phi}{kT}\ell nA(\frac{m^*}{m})T^2$, from which ϕ can be computed. A correction for image force lowering of the barrier height must be made if the semiconductor is heavily doped. The magnitude of the image force correction is $\Delta_{SL}=\frac{1}{\epsilon}\sqrt{\frac{8\phi C(0)}{2\pi A_J}}$, where C(0) is the zero bias capacitance of the depletion region, and A_J is the area of the device.

In reality, the effective ϕ is a slight function of voltage (due to image force lowering), and other current mechanisms contribute to

the observed current. An empirical form for the current-voltage characteristic is then used to show these deviations from ideal thermionic emission current:

$$J = A(\frac{m^*}{m}) \, T^2 \, e^{-\phi/kT}(e^{qV/nkT}-1) \quad ,$$

where n is known as the ideality factor. n varies between 1 and 2, and one can have confidence in the barrier height determined by current-voltage measurements only if n is close to 1.0.

The capacitance-voltage technique can easily be used to determine the barrier height if the doping in the depletion region is fairly uniform, and there are no interfacial impurity layers which can become charged. Then

$$\frac{1}{C^2} = \frac{2(V_{bi} - V - \frac{kT}{q})}{q\varepsilon \, N_D}$$

where

$$V_{bi} = \phi - \frac{kT}{q} \ell n \, \frac{N_D}{N_C}$$

for n-type semiconductors. Substitute $\frac{N_A}{N_V}$ for $\frac{N_D}{N_C}$ on p-type materials. N_D and N_A are bulk carrier concentrations and N_C and N_V are effective conduction and valence band densities of states. C is the capacitance per unit area of the diode and V is the applied voltage across it. A plot of $\frac{1}{C^2}$ vs V should show a straight line characteristic. The

barrier height can be found from the extrapolation to infinite capacitance, and the bulk carrier concentration can be deduced from the slope of the line. Any interfacial layers, or traps in the semiconductor bulk can produce erroneous C-V results, especially in the barrier height determination. For this reason, C-V results must be backed up by I-V or photoresponse before they are to be relied upon.

The photoresponse technique uses the dependence on photon energy of the photoemission of electrons (or holes) from the metal over the barrier into the semiconductor. A plot of $\sqrt{R}$ vs $h\nu$, where R is the short circuit photocurrent per incident photon, usually is a straight line which can be extrapolated to R=0, where $h\nu=\phi-\Delta_{SL}$. Dependencies other than the square root response are predicted for some theoretical models, and are sometimes observed. For the experiments detailed in this chapter, only the square root response plot is used.

The photoresponse measurement is made by illuminating the sample with chopped monochromatic light from a quartz prism monochromator. The induced photocurrent in the Schottky diode is detected synchronously with a lock-in amplifier. The relative photon flux at each wavelength was determined with a thermopile detector that has a flat spectral response. This was used to normalize the signal to incident photon

flux. Whenever possible, the Schottky diode was illuminated through the back of the semiconductor, so that scattered above bandgap light from the monochromator is filtered by the bulk semiconductor. Ohmic contacts were made to the side of the substrates to allow this back-side illumination.

Current-voltage measurement on the evaporated HgSe Schottky barrier diodes did not show pure thermionic emission current; the quality factor was usually about 1.5. Nevertheless, semiquantitative evaluation of the barrier height does yield values which are consistent with C-V and photoresponse measurements.

The first HgSe experiments were performed on ZnS and ZnSe because these materials exhibit large changes in Schottky barrier height with metals of different electronegativity. On ZnS, the barrier height is proportional to the metal electronegativity (Pauling scale) with a slope, S, of one. On ZnSe, S is smaller, about 0.5. In addition, gold Schottky barriers on these materials show nearly ideal I-V, C-V and photoresponse characteristics on samples cleaved in air, with barrier heights which are the same as vacuum-cleaved values. Techniques for preparation of the substrate materials are given in Appendix II.

Typical C-V data for HgSe on both ZnS and ZnSe are shown in Fig. 4. The barrier is determined by adding a correction for the
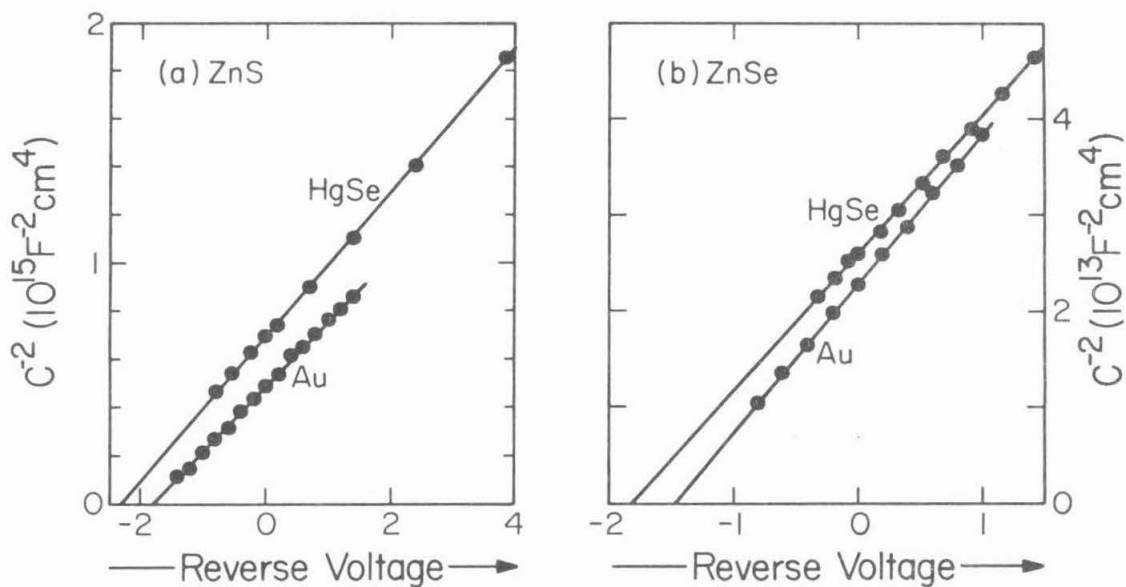
Figure 4. Capacitance-voltage plots of HgSe and Au Schottky barrier data. The voltage intercept plus a small correction gives the barrier energy. The Au data in this figure were provided by R. A. Scranton.

diffusion potential to the voltage intercept of the data for the junction. The range of values determined from data taken on several samples is given in Table I. This represents the extreme range of values measured. The average values were in the middle of these ranges and probably certain to within about 0.1 eV. The data are presented in this manner because the distribution of measured values was not a normal distribution, but more of a flat distribution within the ranges of values given in the table. These values are to be compared with established Au Schottky barrier heights of 1.9-2.0 eV on ZnS and 1.35 eV on ZnSe [12]. Barriers determined by the C-V method on different ZnS samples were spread over a fairly wide range, indicating the effects of an interfacial layer. On ZnSe, C-V data were more consistent, and therefore taken to be more reliable.

Photoresponse curves for HgSe on ZnS and ZnSe are presented in Fig. 5. Using this collection of data, which is also summarized for all samples in Table I, we are able to better define the HgSe on ZnS barrier to be roughly 2.4 eV, 0.4 to 0.5 eV higher than for Au. The data for ZnSe show two distinct slopes. Extrapolating the high energy data to zero response, we obtain a barrier energy of 2.0 eV for HgSe on ZnSe. Extrapolation of the low energy data for ZnSe yields values of the barrier energy which were still larger than those obtained for Au on ZnSe but were inconsistent with the

TABLE I. The range of measured barrier energies (in eV) on
various samples of HgSe on ZnS and ZnSe.

	ZnS	ZnSe
C-V	2.3 - 2.7	1.9 - 2.0
Photoresponse	2.5 - 2.7	2.0 - 2.1
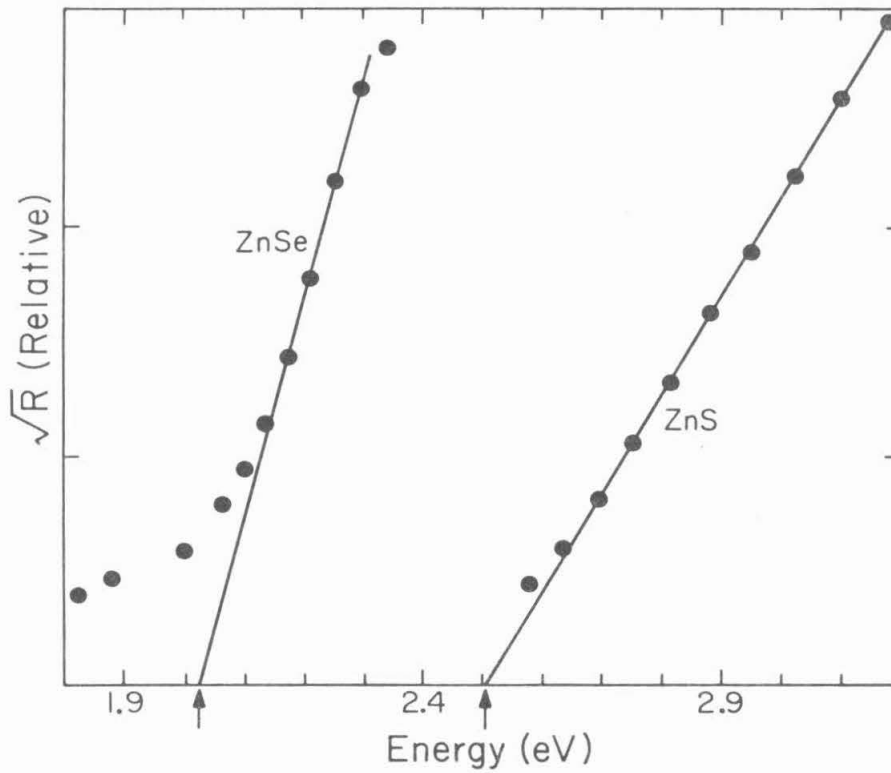
Figure 5. Photoresponse determination of HgSe barrier energy. An extrapolation of the square root of short circuit photocurrent vs photo energy is used to obtain the barrier energies shown by the arrows.

values obtained from the C-V data.

C-V and photoresponse data for HgSe on both n-ZnS and n-ZnSe
show the Schottky barrier energies for these interfaces to be about
0.5 eV larger than Au-semiconductor barriers on the same substrates.
Based upon an S value of 1, we can therefore assign an effective
electronegativity for HgSe of about 2.9 on the Pauling scale, 0.5
larger than Au.

HgSe was also deposited on a variety of other III-V and II-VI
semiconductors. The barrier height improvement on these more covalently
bonded compounds was generally much smaller than on ZnS and ZnSe,
and the data were less reproducible. Results of measurements on some
of these materials, along with those for ZnS and ZnSe, are presented
in Fig. 6.   The shaded regions indicate the extreme ranges of the
measured barrier heights on the different samples. This range is
due to both sample to sample variations and to uncertainties resulting
from nonideality of the C-V, I-V, and photoresponse characteristics.
In some cases, such as for HgSe on GaAs and CdSe, the uncertainty
in the barrier height was about as large as the change with respect
to the gold barrier height.
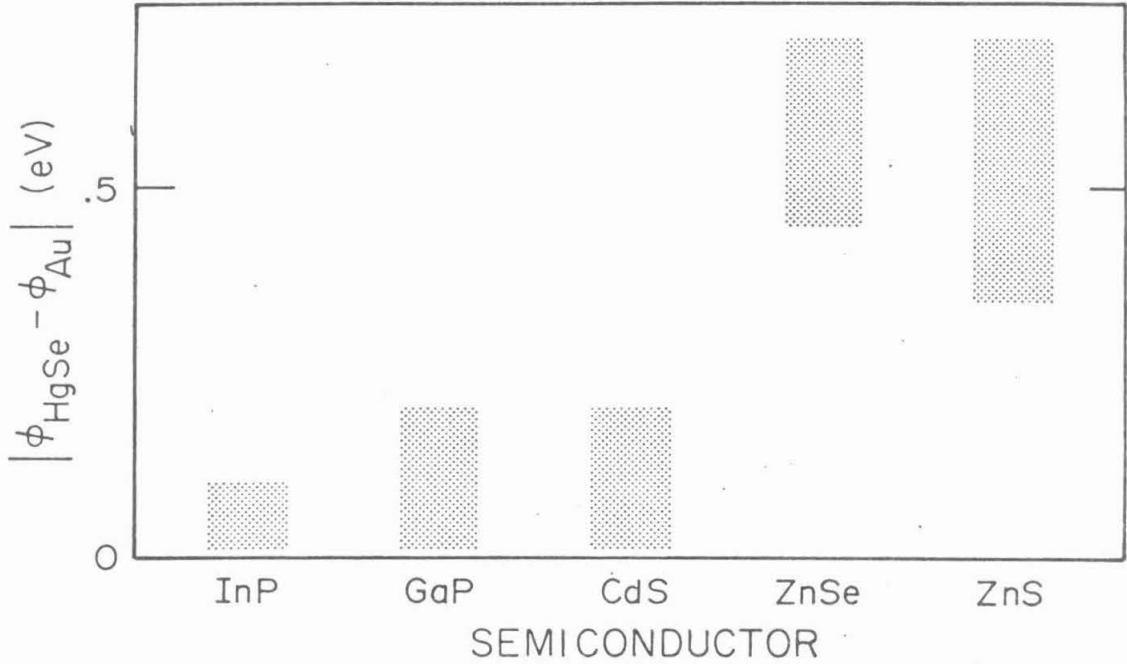
Figure 6. The difference in barrier heights for Au and for HgSe on common compound semiconductors. The shaded regions indicate the extremes of uncertainty of the barrier height measurements. HgSe produces higher barriers to n-type semiconductors and lower barriers to p-type semiconductors than any elemental metal.

D. Discussion

HgSe Schottky barriers follow the general trend of the ionic-covalent transition; the difference between the HgSe and gold barrier heights is large on the very ionic semiconductors, and small on the covalent semiconductors. The mechanism for pinning of the Fermi level on the surface of the covalently bonded semiconductors is not changed by replacing the metal with HgSe. Because the samples were exposed to air before deposition, and the evaporative deposition procedure is not very different from metal deposition, the interactions at the semiconductor surface as the first few atomic layers are deposited are likely to be the same as in metal Schottky formation. The barrier height on the covalent semiconductors appears to be almost completely determined as the first monolayer of metal or impurity condenses on the sample [13], hence the HgSe results are not surprising. Schottky barriers formed with the other highly electronegative contact that has been found, $(SN)_x$, also follow the ionic-covalent transition [14].

If the evaporated HgSe contact is to be used for practical device applications, some further refinement in the deposition procedure will be necessary. More reproducible Schottky barrier characteristics could probably be obtained by providing better control over the selenium evaporation rate and the mercury pressure. A controlled, elevated substrate temperature (perhaps 100 to 150°C) might also contribute to more uniform, pure and stoichiometric HgSe layers.

Some effort was made to adapt this deposition method for epitaxial growth of HgSe on CdSe. The high vapor pressure of both mercury and selenium over HgSe at temperatures over $200^{o}C$ make such growth difficult. Epitaxial growth should be possible with a more elaborate apparatus than described here, especially with regard to the mercury source.

In summary, evaporated HgSe thin films provide larger barriers to n-type semiconductors and lower barriers to p-type semiconductors than do the elemental metals. On n-ZnSe and n-ZnS, the HgSe barrier height is 0.5 eV greater than the gold barrier; on more covalently bonded semiconductors, the difference is smaller. This is consistent with the ionic covalent transition noted by Kurtin, McGill and Mead.

REFERENCES

1. V. Marrello, W. Rühle, A. Onton, Appl. Phys. Lett. <u>31</u>, 452
   (1977).

2. D. B. Holt, Thin Solid Films, <u>24</u>, 1 (1974).

3. K. C. Barva and A. Goswami, Jap. J. Appl. Phys. <u>9</u>, 705 (1970).

4. <u>Handbook of Chemistry and Physics</u>, 53rd ed., edited by R.
   Weaste (Chemical Rubber Co., Cleveland, Ohio, 1972) p B131.

5. A. Y. Cho and J. R. Arthur, <u>Progress in Solid State Technology</u>,
   edited by G. A. Somoljai and J. O. McCaldin (Pergamon, Oxford,
   1975) Vol. 10, p 157.

6. <u>Lange's Handbook of Chemistry</u>, 11th edition, edited by John A.
   Dean, (McGraw Hill, New York, 1973), p 10-22.

7. L. Pauling, <u>General Chemistry</u> (W. H. Freeman & Son, San Francisco,
   1970) 3rd ed., p 216.

8. J. Berkowitz and W. A. Chupka, J. Chem. Phys. <u>45</u>, 4301 (1966).

9. C. A. Mead, Solid State Electron., <u>9</u>, 1023 (1966).

10. E. H. Rhoderick, <u>Metal-Semiconductor Contacts</u> (Clarendon,
    Oxford, 1978) pp 46-50.

11. S. M. Sze, <u>Physics of Semiconductor Devices</u>, (Wiley, New York,
    1969), pp 393-410.

12. op. cit., C. A. Mead.

13. I. Lindau, P. W. Chye, C. M. Garner, P. Pianetta, C. Y. Su, and
    W. E. Spicer, J. Vac. Sci. Technol. <u>15</u>, 1332 (1978).

14. R. A. Scranton, J. Appl. Phys. $\underline{48}$, 3838 (1977).

CHAPTER 3

LATTICE MATCHED HgSe/CdSe HETEROSTRUCTURES

AS SCHOTTKY BARRIERS

A. INTRODUCTION

As pointed out in Chapter 1, the structure of the interface between a metal and a semiconductor, as usually fabricated, is complicated. Metal deposition can disrupt the surface of the semiconductor. Bonding on either side of the interface differs drastically and new thermodynamic phases may occur at such interfaces. On the other hand, lattice-matched heterostructures, such as $Ga_{1-x}Al_xAs/$ GaAs, are relatively simple.

The mercury-chalcogenide/cadmium-chalcogenide interface is a unique "Schottky barrier" in that it is also a lattice-matched heterostructure. The tetrahedrally coordinated compounds HgX, where X is S, Se, or Te, are semimetallic, and each has about the same interatomic spacing as the corresponding CdX semiconductor. HgX/CdX interfaces can therefore be grown as lattice-matched heterostructures. CdSe has a hexagonal, wurzite structure. HgSe has a cubic, zincblende structure. The two structures differ in the stacking sequence of hexagonal close packed planes. The spacing between like atoms in a given hexagonal close packed plane is given by the lattice parameter a_0 for wurzite crystals, where the basal plane is the close packed one. In the cubic crystal, the <111> planes are hexagonal close packed and the spacing between like atoms is $a_0/\sqrt{2}$. A good lattice match can therefore be achieved between a wurzite type basal <0001>

plane and a zincblende type <111> plane if $\sqrt{2}$ a_0 (wurzite) = a_0 (zincblende). Referring to Appendix I , $\sqrt{2}$ a_0 for CdSe is 6.079 Å and a_0 for HgSe is 6.084 Å, a mismatch of only 0.08%. Small mismatches also occur for HgTe/CdTe and β-HgS/CdS heterostructures. Thus, the HgX provides a Schottky-like contact to the CdX without the structural complexity that causes difficulty in understanding metal-semiconductor interfaces.

HgSe epitaxial growth was achieved using hydrogen transport chemical vapor deposition (CVD). The deposition takes place slowly, under near equilibrium conditions, which allows the growth of good quality, high purity epitaxial layers. The basic scheme for this type of growth is to pass hydrogen gas in a tube furnace over a polycrystalline source of the material to be deposited. The HgSe is then transported as Hg vapor and H_2Se, as the H_2 reacts with the HgSe according to the reaction $H_2 + HgSe \rightleftarrows H_2Se + Hg$. Downstream in the gas flow, the furnace temperature is lower and this reaction is reversed, depositing HgSe on the sample. By examining the equilibrium thermodynamics of this reaction, we can determine how much HgSe is transported in the ideal equilibrium case. The free energy change for this reaction is given for various temperatures in Appendix III. From this, the equilibrium quantity of HgSe transported can be computed, using

$$\frac{[H_2Se]\,[Hg]}{[H_2]\,[HgSe]} = e^{-\Delta G/kT} \qquad .$$

[H_2Se], etc. represent the concentrations of the various constituents. Since ΔG has been computed at one atmosphere of pressure, these concentrations for the gaseous components are the partial pressures in atmospheres. [H_2Se], for the solid HgSe, is one. Since the CVD furnace is operated with pure H_2 at one atmosphere, [H_2] is also one, and [H_2Se] = [Hg] because the only source for both is the HgSe. Therefore,

$$[H_2Se]^2 = [Hg]^2 = e^{-\Delta G/kT} \quad .$$

For the growth temperature used, 420°C, ΔG is 7.3 kcal/mole, so $e^{-\Delta G/kT}$ is 4.95×10^{-3} and [Hg] is 7.0×10^{-2}. For the 330°C substrate temperature, ΔG is 10.6 kcal/mole, $e^{-\Delta G/kT}$ is 1.42×10^{-4}, and [Hg] is 1.2×10^{-2}. Using PV = NRT, the number of moles per liter of H_2 removed from the source is 1.2×10^{-3}, and the amount remaining in the gas phase at the substrate position is 2.4×10^{-4} moles/liter. At a gas flow rate of 8 ml/sec, this makes ≈ 8.0 gr/hr of HgSe available for deposition. In actual fact, the gas is not saturated at the position of the source, although it must be at the substrate for growth to take place; and the Hg and H_2Se concentration is probably not completely uniform across the diameter of the furnace tube. As a result, the actual transport rate (unmeasured) is probably one or two grams per hour.

An important consideration in the growth of this heterostructure

is the amount of interdiffusion between the CdSe substrate and the HgSe epitaxial layer. If the interdiffusion distance is of a magnitude compared with the Debye length in the CdSe, the potential difference is screened out by the mobile charge in the semiconductor, and no barrier is seen. More exactly, Oldham and Milnes [1] have shown that for rectification in an n-n heterojunction to occur, the interdiffusion distance $\sqrt{Dt}$ must be less than $L_D(\Delta\chi/10kT)^{1/2}$, where $\Delta\chi$ is the conduction band discontinuity for the ideal abrupt junction and L_D is the Debye length, $(kT\varepsilon/q^2N_D)^{1/2}$ in the semiconductor in which the band bending takes place. For our case, $\varepsilon\approx10$ $\Delta\chi\approx0.7$ eV (from results), and $N_D\approx10^{15}cm^{-3}$, so the requirement is $\sqrt{Dt}$ < 1960 $\overset{o}{A}$. For a $\sqrt{Dt}$ of one-tenth of this, little decrease in the barrier height from the ideal case would be expected.

Interdiffusion data for the HgSe/CdSe system are not available The HgTe/CdTe system has been extensively studied, so that a rough guess as to the interdiffusion rate for HgSe/CdSe can be made. Almasi and Smith [2] performed interdiffusion experiments in the temperature range of 450 to 630°C. Extrapolating to 315°C, $\sqrt{Dt}$ $\approx$ 100 $\overset{o}{A}$ for a growth time of one hour. This is small enough that little reduction of the barrier should occur. Measured barrier heights, to be described, were fairly independent of the exact growth time and temperature, indicating that this conclusion is probably correct. Samples grown on CdSe with a large carrier concentra-

tion ($\gtrsim 10^{17} cm^{-3}$) have a much shorter Debye length, and did not exhibit rectifying characteristics. Tunneling through the narrow depletion region may contribute to this behavior.

B. EXPERIMENTAL EQUIPMENT

The CVD furnace setup is schematically illustrated in Fig. 1 It consists of a 1 1/2" diameter two zone furnace, with each zone independently controllable. During growth, the HgSe source sits in an open boat in the lefthand zone. The sample sits on a quartz paddle in the righthand zone at a temperature lower than the source. Both the source and sample positions in the furnace can be independently controlled by moving the 7 mm o.d. quartz tubes to which they are connected. Thermocouples are placed in the quartz tubes, where they can monitor the source and sample temperatures without being exposed to the furnace gases.

H_2 and Ar are fed into the furnace through a ground glass taper joint connection on the furnace tube that is sealed with black wax. Prepurified grade (99.99% H_2 or 99.998% Ar) gases were used. The H_2 was passed through a catalytic purifier and LN_2 trap to remove oxygen and water vapor.

During early phases of the work, oxygen in the CVD furnace caused some problems; in particular, the formation of a black deposit on the CdSe during the substrate etching phase of the growth

$$HgSe + H_2 \rightleftharpoons H_2Se + Hg$$
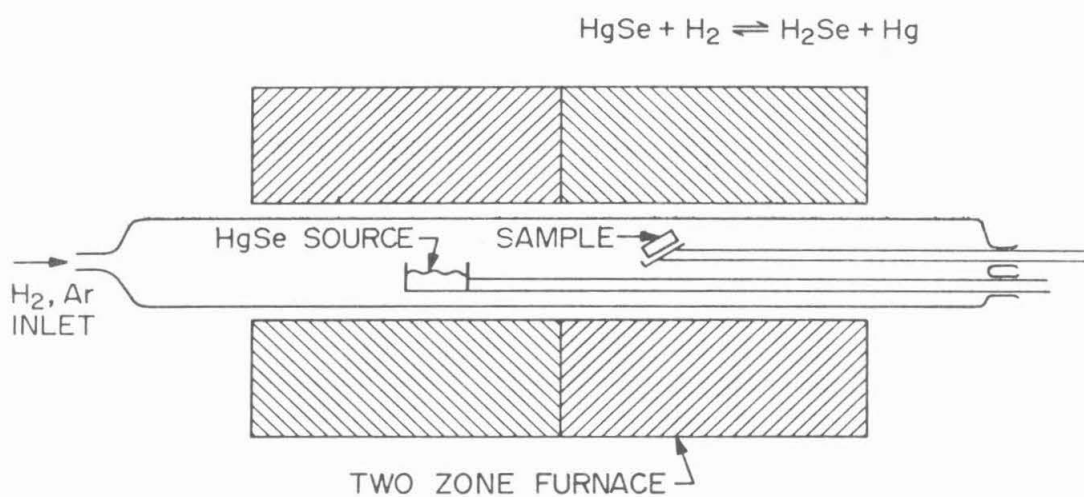
Fig. 1. Schematic diagram of the two zone furnace used for H_2 transport CVD of HgSe on n-CdSe. The source and sample holder rods can be independently moved within the furnace. All hardware exposed to the carrier gas is made of quartz or teflon.

procedure. In light of this, a discussion of oxygen content in the furnace follows.

Oxidation of a metal, such as Cd, can occur, even in a reducing atmosphere of mostly hydrogen if the water content of the hydrogen is greater than the value for equilibrium with the metal and its oxide. Consider the reaction $(A)H_2O+(B)M \underset{\rightleftharpoons}{\overset{\Delta G}{}} M_B O_A+(A)H_2$. Oxidation of M will occur in a hydrogen atmosphere if

$$\frac{[H_2O]^A}{[H_2]^A} \geq e^{\Delta G/kT} \quad .$$

In Appendix III, this ratio has been calculated for a number of metals at various temperatures. For the case of cadmium, a very large water content can be tolerated without oxidation. There are a number of other compounds, such as cadmium selenate or selenium oxides, which are more stable than CdO. For this reason, it is still necessary to keep the water concentration in the furnace at a fairly low level ($\approx$100 ppm).

Given that the incoming gas is pure, the major source of oxygen in the tube furnace is back diffusion from the exhaust end of the furnace. Consider first a very simplified model for gas flow in the furnace, with a constant and uniform flow velocity across the diameter of the furnace tube. For the flow rates and tube diameter used here, the average linear flow rate for the gas in the furnace is

about 1 cm/sec. Consider the steady state solution of the diffusion equation with a fixed oxygen concentration at the end of an open furnace tube. The diffusion equation,

$$D \frac{\partial^2 C}{\partial x^2} = \frac{\partial C}{\partial t}$$

becomes

$$D \frac{\partial^2 C(x-vt)}{\partial (x-vt)^2} = \frac{\partial C(x-vt)}{\partial t}$$

for a flow moving at velocity v. Using the chain rule for derivatives, the equation becomes

$$D \left[\frac{\partial^2 C}{\partial x^2} - \frac{2}{v} \frac{\partial^2 C}{\partial x \partial t} + \frac{1}{v^2} \frac{\partial^2 C}{\partial t^2} \right] = v \frac{\partial C}{\partial x} + \frac{\partial C}{\partial t}$$

In the steady state, all derivatives in t vanish, so

$$D \frac{\partial^2 C}{\partial x^2} = v \frac{\partial C}{\partial x}$$

The general solution is

$$C = Ae^{\frac{vx}{D}} + B$$

The boundary conditions are $C(0) = C_o$, and $C(-\infty) = 0$, so $C(x) = C_o e^{vx/D}$, where the end of the furnace tube is at x=0. For a flow velocity of about 1 cm/sec, and D of 1, the oxygen concentration will fall off to 100 ppm at a distance of 9 cm into the tube.

In actual fact, the flow rate is not constant across the diameter of the tube. For laminar flow in a pipe, the velocity is zero at the walls, and increases toward the center according to the flow equation

$$\frac{\partial^2 v}{\partial y^2} + \frac{\partial^2 v}{\partial z^2} = \frac{1}{\eta} \frac{dP}{dx} \quad ,$$

where v is the flow velocity, η is the vicosity, and P is the pressure. In cylindrical co-ordinates, this becomes

$$\frac{1}{r} \frac{d}{dr} \left(r\frac{dv}{dr} \right) = - \frac{\partial P}{\eta \partial x} \quad .$$

Then,

$$v = \left(\frac{\partial P}{\partial x}\right) \frac{1}{4\eta} (R^2 - r^2) \quad ,$$

where R is the pipe radius. This can also be expressed as

$$v = 2v_{av}\left(1 - \frac{r^2}{R^2}\right),$$

where v_{av} is the average flow velocity. The Reynolds number, $R_e = \rho v \ell / \eta$, where ρ is the density and ℓ is a characteristic dimension of the object through which flow is taking place, is about 1 for the CVD furnace, so laminar flow is expected ($R \leq 10$ is usually laminar flow) [3]. The stalled flow near the tube boundary would allow oxygen to diffuse farther back into the tube furnace than the 9 cm mentioned above. Finally, convection currents due to temperature

differences in the furnace probably cause a great deal of gas mixing in the furnace. Quartz wool stuffed into the end of the furnace to prevent convection currents from mixing outside air with the gas in the furnace is not sufficient to keep oxygen out of the furnace because diffusion alone can carry significant concentrations through at least 9 cm of quartz wool.

To keep oxygen from the inside of the tube, the exhaust end was capped with a quartz end cap sealed with a ground glass taper joint and black wax. The sample and source holder quartz tubes passed through close fitting teflon sleeves in the end cap. Ar or H_2 exhaust passes at high velocity between the teflon sleeves and the quartz. The oxygen concentration is kept well under 100 ppm with this apparatus.

C. SAMPLE PREPARATION

Substrates were prepared from an undoped CdSe boule obtained from Eagle Pitcher. The boule was hand oriented close to <0001> orientation by observing the orientation of <10$\bar{1}$0> and <11$\bar{2}$0> prism cleavage faces. Using this as a guide, the boule was oriented and sliced to within 0.5^o of <0001> using Laue back reflection X-ray photographs. X-ray exposure was for 1 1/2 hours with a 3 cm sample to film distance and using a Mo target x-ray tube operated at 23 kV and 20 mA.

The slices were lapped against a flat glass plate, using 800, 1200, and 3200 mesh carborundum, followed by 1 and 0.25 micron diamond paste. During this procedure, the CdSe was waxed to the end of a brass cylinder which was held accurately parallel to the glass plate. The samples were then cleaned in TCE, acetone, and methanol, while rubbing with a Q-tip to remove any remaining polishing compound. Work damage was removed by etching in 5% bromine-methanol solution for 5-7 minutes, while occasionally rubbing with a Q-tip to remove surface deposits. Finally, the sample was polished in 0.5% bromine-methanol for about one minute while rubbing on a piece of Texwipe Corporation "Microwipe" cloth.

The resulting surface after this procedure is not perfectly flat, but it is smooth on a scale of a few microns and is free of significant work damage. Samples prepared without sufficient bromine-methanol etching show many hillocks on the grown HgSe surface due to defects left in the substrate from the mechanical lapping.

Within a few minutes after polishing, the substrates were loaded into the furnace tube, but held outside of the furnace itself, and Ar gas flow was initiated. The furnace controller was then set to the desired temperatures for the etching phase of the growth: $420^{o}C$ for the source zone (zone 1) and $575^{o}C$ for the sample zone (zone 2). After allowing the furnace temperature to stabilize, the sample

was pushed to the center of the sample zone of the furnace. After etching for a period of 30 minutes, the CdSe was pushed to a position close to zone 1 of the furnace, but still in the flat part of zone 2 temperature profile. This position, marked in Fig. 2 , is the position of the sample for growth. Because shunt taps on the furnace windings were adjusted for an abrupt temperature change between the two zones when zone 1 is hotter than zone 2, the temperature at this position is about 100^oC cooler than the middle of zone 2 during the etch phase of the procedure. The actual etching of the sample therefore terminates when the sample is moved, even though it takes about 2 1/2 hours for the furnace to stabilize at the new zone 2 temperature of 330^oC.

The total amount of etching of the CdSe substrate was small - less than 1000 $\overset{o}{A}$. The primary purpose of this step was to clean the surface, not to provide significant etching of the CdSe. The HgSe growth morphology is very poor if this step is not performed, with nucleation and growth occurring only in patches on the CdSe surface.

This substrate cleaning can also be performed in pure H_2; however, this causes the CdSe surface carrier concentration to become too high for barrier measurements. The extreme reducing atmosphere shifts the CdSe stoichiometry to the cadmium rich side of the CdSe phase stability region, and Cd interstitials or Se vacancies
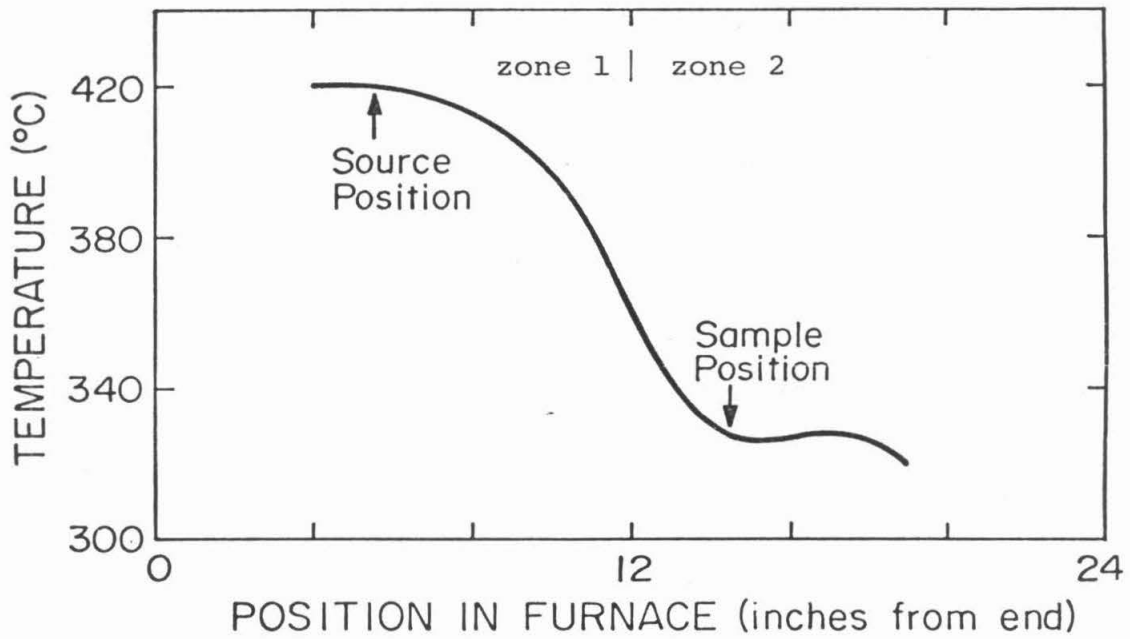
Fig. 2. Temperature profile of the furnace during the growth. The arrows indicate the positions of the polycrystalline HgSe source and the CdSe substrate.

act as donors to make the material heavily n-type. The inter-
diffusion between the HgSe and CdSe, combined with tunneling through
the narrow barrier in the heavily doped CdSe, cause the diodes on H_2
etched CdSe to have ohmic characteristics.

During the etching step, the furnace gas was changed to H_2 and
the source was pulled into zone 1 of the furnace. Growth times of
from 10 minutes to 5 hours were used for various samples. Resulting
HgSe layers were from 800 nm to tens of microns thick. After the
growth step, the samples were immediately pulled from the furnace
to prevent thermal decomposition of the HgSe layer during cooling
of the furnace.

D. GROWTH PROPERTIES

The surface morphology of the HgSe layers is illustrated in
Fig. 3. The surface typically consisted of a series of flat terraces.
The steps between terraces were aligned in relation to the misorienta-
tion of the CdSe from true basal plane, so that the terrace surfaces
were true (111) planes of the HgSe. The height and distance be-
tween the steps increases with increasing growth thickness. The
particular sample shown in Fig. 2 was one of the thinner epi growths.
Terraces up to almost 1 mm across have been observed after long
growth times on well oriented substrates.
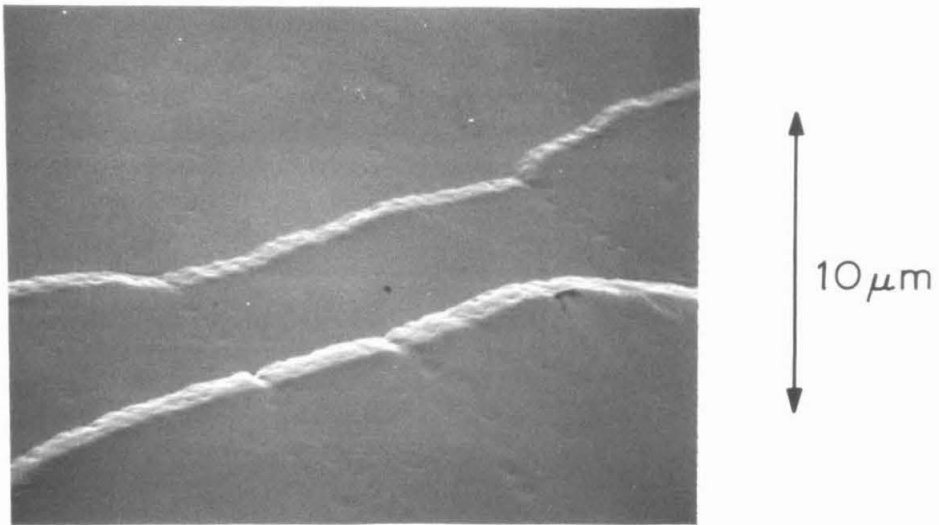
Fig. 3. SEM photograph of HgSe epitaxial layer surface.

The cleaved edge in Fig. 4 shows that the HgSe layer is uniform
and contains no macroscopic voids. The interface is smooth and
looks abrupt on this scale. Cleavages through terrace steps show
that the steps range in height up to about one-third of the total
thickness of the HgSe layer.

The <0001> faces of CdSe are polar, one face terminating in Cd,
the other in Se. Growth was attempted on both the A, or "Cd" face
and the B, or "Se" face of the CdSe. The two faces were distinguished
before growth by their etching characteristics in HCl solution.
The A face remains smooth after the etch, but becomes brownish in
color; the B face is roughened by the etch and is less discolored [4].
Figs. 3 and 4 are of HgSe grown on the A face. Growth on the B
face consisted of many triangular hillocks, and was not used for
further measurements.

Figure 5 shows 1.5 MeV ^{4}He$^+$ ion Rutherford backscatter spectra
for (111) aligned and randomly oriented HgSe layers. The back-
scattering yield for a beam of ^{4}He$^+$ ions impinging on a well aligned
perfect crystal is very low (a few percent of the yield for a ran-
domly aligned crystal), because the ions are channeled between the
rows of atoms in the crystal [5]. The reader not familiar with back-
scatter technique should consult reference (5) for more details of
the principles involved. The data indicate that the layer is
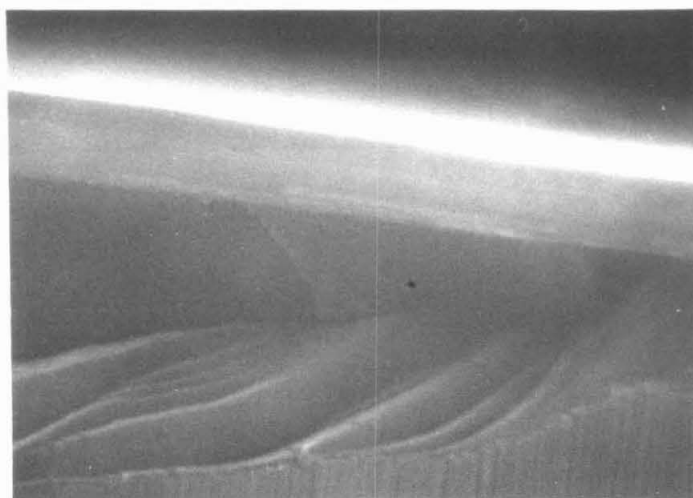
Fig. 4. SEM photograph of a cleaved cross section of HgSe on CdSe. The very bright, narrow region is the surface of the HgSe epi layer. Below that is the ≈8000 Å thick, uniform HgSe layer. The lower 60% of the figure is the CdSe substrate.
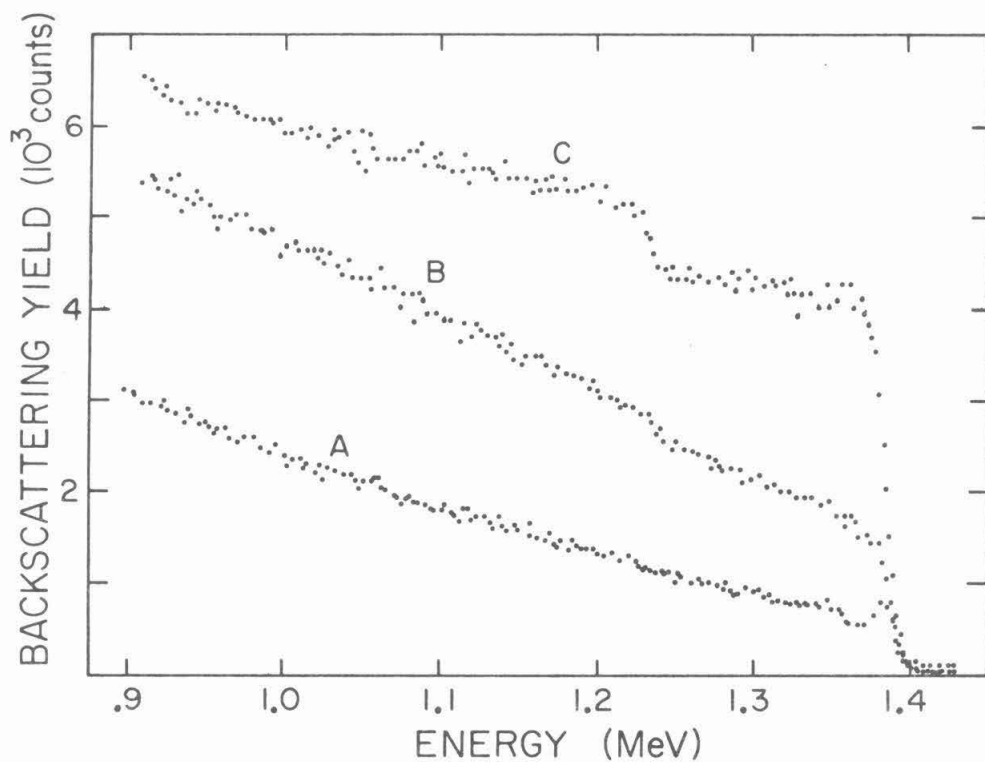
Fig. 5. 1.5 meV ^{4}He$^+$ channeling spectrum for HgSe epitaxial layer.
Curve A is (111) aligned on well-oriented substrate. Curve B is
(111) aligned on 2° misoriented substrate. Curve C is randomly
aligned.

indeed epitaxial single-crystal. The (111) aligned channeling minimum yield is 15%, indicating that some defects, possibly dislocations, are present. The channeling spectrum for a sample grown on a substrate intentionally misoriented by 2° is also shown, and the minimum yield is about 40%. The small peak in the yield at the high energy end of Curve A is due to backscattering from the atoms at the surface of the crystal. The surface peak in curve B is also not evident, indicating poor epitaxy. Continuous films of HgSe are difficult to obtain on substrates misoriented by 3° or more.

There are two equivalent, but different orientations in which the three-fold symmetric (111) planes of HgSe can grow on the six-fold CdSe basal plane. These differ in the order of the stacking sequence of the hexagonal close packed (111) planes. Equivalently, they differ by a 60° rotation about the [111] axis. The Laue back reflection x-ray pattern in Fig. 6 shows the three-fold symmetric pattern of the zincblende structure (111) plane. The three-fold symmetry indicates that only one of the two possible HgSe orientations is present. This was true of all samples on which a Laue pattern was obtained.

Some property of the bulk CdSe, of the substrate preparation, or of the growth itself has caused a breaking of the six-fold symmetry seen by the HgSe as the epitaxial layer grows. Attempts to correlate
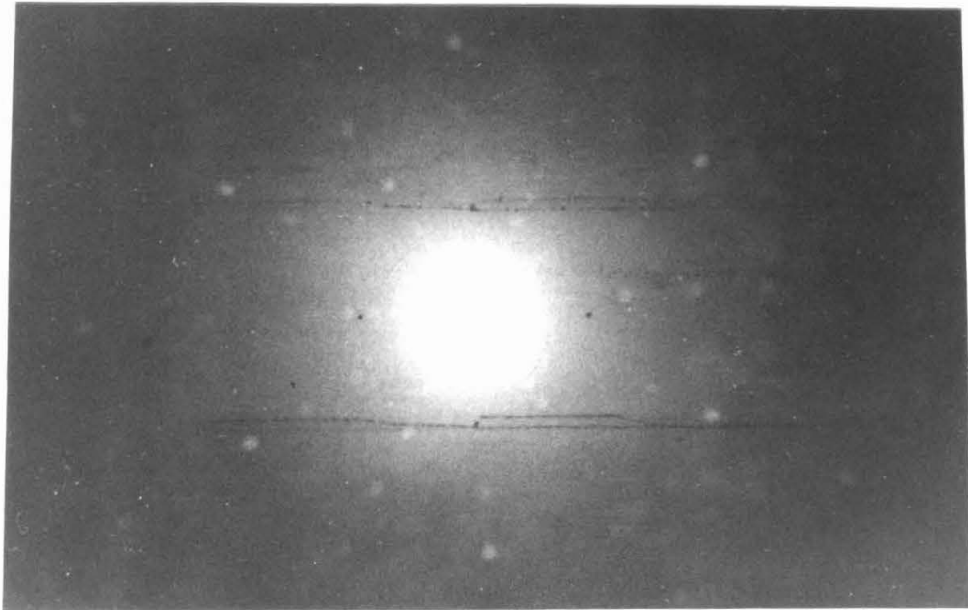
Fig. 6. Laue back reflection x-ray photograph of HgSe epi layer. Close examination of the photo reveals the 3-fold symmetry of the (111) oriented HgSe.

the orientation of the HgSe with the small misorientation ($\approx$ 0.5 degrees) of the substrate have been unsuccessful. Another possible cause is defects in the CdSe substrate.

E. ELECTRICAL MEASUREMENTS

Grown samples were prepared for electrical measurements by masking with black wax and etching mesas with bromine-methanol solution. The mesa area was between 1×10^{-4} and $3 \times 10^{-3} (cm)^2$. Ohmic contacts were made to the substrates with In-Ag solder. Traditional techniques of current-voltage and photoresponse were used to measure the Schottky barrier heights. The capacitance-voltage technique was not useful for measuring the barrier height of either HgSe or gold on CdSe due to large numbers of traps in the CdSe.

Current-voltage curves are shown in Fig. 7, along with Au on n-CdSe Schottky barrier data for comparison. For pure thermionic emission current at room temperature, the slope of the curves should be about 1 decade of current change for each 60 mV increment of bias. The Au on bromine-methanol etched CdSe diodes show a less than ideal slope. A cleaner, Au on air-cleaved CdSe interface shows the ideal slope, and a barrier height of 0.5 eV which is the same as the vacuum-cleaved value [6]. The HgSe data shown has a slope close to the ideal value and a barrier height of 0.73 eV.
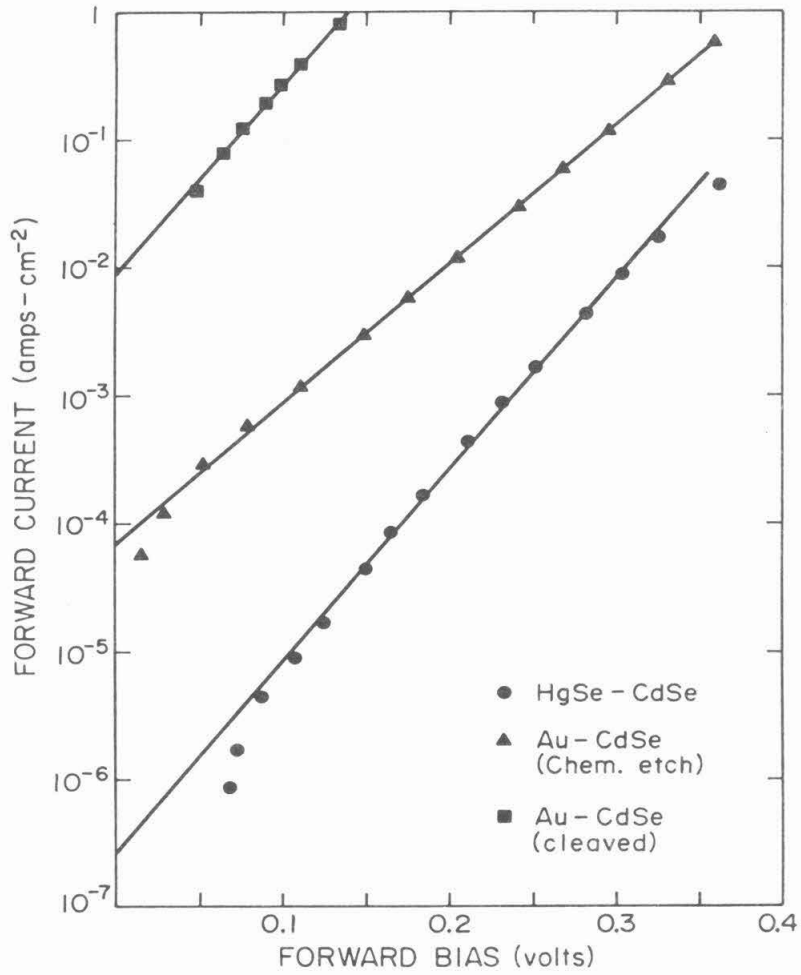
Fig. 7. Current voltage characteristics for HgSe on n-CdSe and Au on n-CdSe Schottky barrier diodes. The barrier height for the HgSe/CdSe curve shown is 0.73 eV.

Most HgSe diodes have an excess, non-thermionic emission current, which produces an I-V characteristic between that of the HgSe sample shown and the Au on chem-etched CdSe sample, both in slope and in magnitude. Leakage at the etched mesa periphery and defects at the heterostructure interface are possible sources of this current. The barrier height, as estimated using thermionic emission theory, is always greater than 0.6 eV.

Photoresponse data are shown in Fig. 8. For HgSe on CdSe internal photoresponse, the photocurrent per incident photon, R, increases linearly with $(h\nu)^3$. A square law is usually observed for metal-semiconductor Schottky barriers. This cube law is typical of photoemission from semiconductors into vacuum near the threshold for emission [7]. The evaporated HgSe layers, which did not have the macroscopic crystallinity of CVD grown HgSe, exhibited a square law response.

The Schottky barrier height deduced from the photoresponse measurements is 0.73 ± 0.02 eV. It is reproducible even on samples which do not have ideal current-voltage characterisitcs. This number is probably the energy of the top of the HgSe valence band with respect to the bottom of the CdSe conduction band at the interface. It is not the Fermi level position normally measured by photoresponse, as the HgSe Fermi level is about 0.1 eV above the
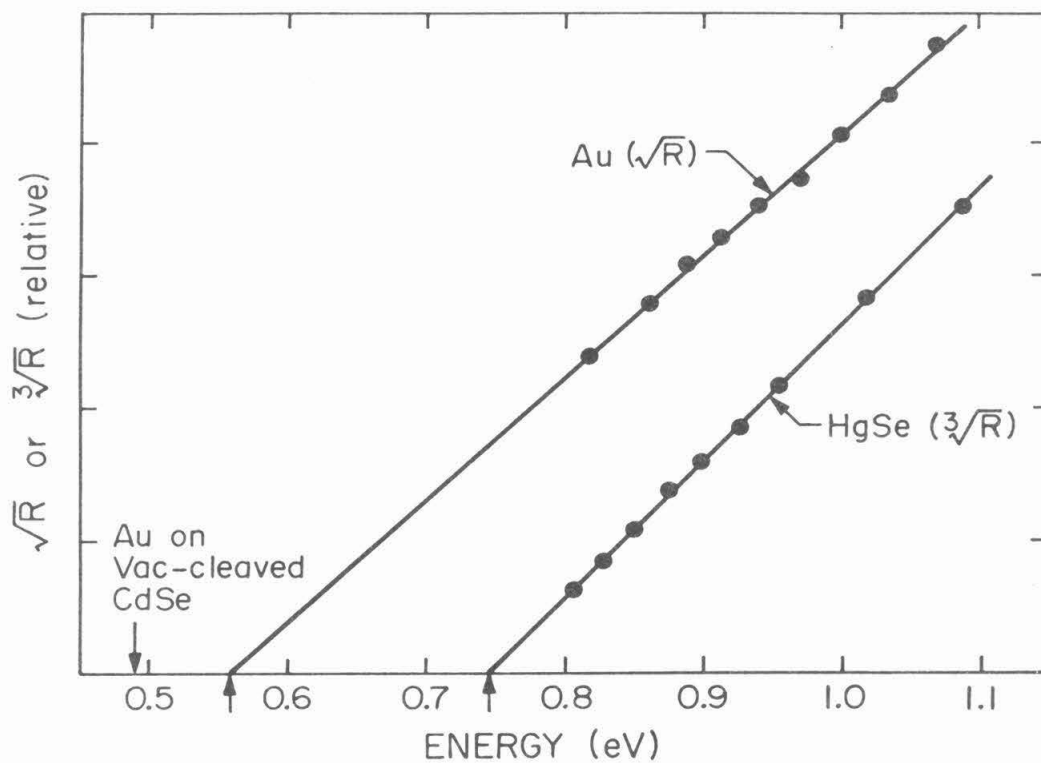
Fig. 8. Photoresponse measurements of HgSe on n-CdSe and Au on chemically etched n-CdSe Schottky diodes.

valence band maximum/conduction band minimum.

A few HgSe on n-CdSe samples were also made using the evaporation technique of Chapter 2. These polycrystalline HgSe on n-CdSe diodes yielded poorly reproducible barrier heights which were comparable with the Au on CdSe values.

F. DISCUSSION

The simple model of the heterostructure interface, combined with an extension of the common anion rule, predicts that the valence band discontinuity in a HgSe/CdSe heterostructure might be close to zero. This would give a Schottky barrier height of almost the full band gap of CdSe, 1.74 eV. This is clearly not the case.

If we examine available vacuum photoemission data for HgSe, it is apparent that bulk HgSe does not have as large an ionization potential as would be expected from the common anion rule. In fact, the ionization potential is about 1.1 eV less than the potential for CdSe [8,9]. The CdSe band gap is 1.74 eV. Therefore, we expect a conduction band discontinuity of 0.64 eV. As the ionization potential data has an uncertainty of a couple of tenths of a volt, this is consistent with the experimental result of 0.73 eV. This conclusion should be viewed with some caution, as the only available

photoemission data for HgSe (Ref. 8) were taken on sputter deposited HgSe films. Such data cannot be trusted to be as reliable as ionization potential measurements on cleaved single crystals.

It is also known that one cannot make CdSe significantly p-type. Compensating defects are created in the crystal as the Fermi level is pushed toward the lower half of the energy gap [10]. This may also prevent one from producing a Schottky barrier on n-CdSe with a barrier height as large as one-half of the band gap.

Neither of the above limitations exists for the case of HgTe on CdTe. The ionization potentials for the two materials are similar [8,9], and CdTe can be made p-type. Both materials are of the zinc-blende structure, resulting in a true lattice-match for any orientation. The CVD technique used for HgSe is not applicable to HgTe, because the H_2 transport takes place at higher temperatures, when the mercury pressure over the HgTe becomes excessive. Therefore, thermal decomposition of source takes place, with only Hg vapor being transported [11]. Given that a suitable growth technique can be found, future measurements on the HgTe/CdTe system should prove to be very interesting.

In summary, simple, straightforward CVD techniques have been used to grow a lattice-matched heterostructure which is also a

Schottky barrier. It has a much simpler interface structure than conventional metal-semiconductor Schottky barriers. The structure shows an exceptionally reproducible barrier height which is consistent with that predicted from a simple application of available ionization potential data for the bulk semiconductors. In addition, the barrier height is larger than that of any elemental metal on n-CdSe.

REFERENCES

1. W. C. Oldham and A. G. Milnes, Solid State Electron. $\underline{6}$, 121 (1963).

2. G. S. Almasi and A. C. Smith, J. Appl. Phys. $\underline{39}$, 233 (1968).

3. L. D. Landau and E. M. Lifshitz, Fluid Mechanics, (Pergamon, Oxford, 1959) p 103.

4. W. H. Strehlow, J. Appl. Phys. $\underline{40}$, 2928 (1969).

5. W. K. Chu, J. W. Mayer and M-A. Nicolet, Backscattering Spectrometry, (Academic Press, New York, 1978), Ch. 8.

6. C. A. Mead, Solid State Electron. $\underline{9}$, 1023 (1966).

7. J. I. Pankove, Optical Processes in Semiconductors, (Prentice-Hall, Englewood Cliffs, N.J. 1971), p 290.

8. N. J. Shevchik, J. Tejeda, M. Cardona and D. W. Lander, Phys. Stat. Sol.(b), $\underline{59}$, 87 (1973).

9. R. K. Swank, Phys. Rev. $\underline{153}$, 844 (1967).

10. F. A. Kroger, private discussion.

11. T. F. Kuech, private discussion.

CHAPTER 4

Au ON CHEMICALLY ETCHED $Ga_{1-x}Al_xAs$

A. INTRODUCTION

As pointed out in Chapter 1, the gold Schottky barriers on the common III-V and II-VI semiconductors follow a pattern in which the barrier height to p-type semiconductors, ϕ_p, is determined solely by the anion of the semiconductor. The common anion rule has also been tested for two alloy systems, $Ga_xIn_{1-x}As$ [1] and $Ga_xIn_{1-x}P$ [2]. In both cases, the rule works over the entire composition range of the alloy.

The common anion rule fails for some of the III-V and II-VI compounds. Aluminum compounds are the most important examples of this failure. The barrier height for Au on n-GaAs is 0.9 eV. The barrier height for Au on n-AlAs is 1.2 eV, a difference of 0.3 eV [3]. The difference in band gap between the two semiconductors is 0.74 eV. Applying the relationship $\phi_n + \phi_p = E_g$, we see that the difference in barriers to the n-type materials is more than 0.4 eV less than would be predicted from an application of the common-anion rule. A similar failure of the rule occurs for the case of AlSb.

A study of the Au Schottky barrier height on $Ga_{1-x}Al_xAs$ as a function of the AlAs mole fraction, x, is then important for two reasons. First, it would show how the common anion rule fails with increasing aluminum concentration, and possibly why. Second, the

$Ga_{1-x}Al_xAs$ alloy system is extremely important technologically, so that a knowledge of the Schottky barrier heights across the alloy diagram could be useful in building devices. This chapter reports measurements of the barrier heights of Au on $n\text{-}Ga_{1-x}Al_xAs$ for several values of x.

B. SAMPLE PREPARATION

Schottky barriers were fabricated on Sn-doped LPE grown $Ga_{1-x}Al_xAs$ epitaxial layers. The substrate material was (100) oriented Cr-doped, semi-insulating GaAs. The use of the semi-insulating substrate insured that measurement of the Schottky barriers on the epi-layer surface would not be confused with characteristics of the $GaAs/Ga_{1-x}Al_xAs$ heterojunction.

The 5 to 7 micron thick epitaxial layers were n-type with carrier concentration in the range $2x10^{16}cm^{-3}$ to $2x10^{17}cm^{-3}$, as measured by the capacitance-voltage method.

Samples were prepared by first making ohmic contact to a portion of the $Ga_{1-x}Al_xAs$ layer with an88% Au- 12% Ge eutectic alloy. After etching for 30 sec in 15% HCl solution (1 part 30% HCl reagent: 1 part H_2O), the alloy was evaporated through a mask onto a 1 x 1 mm portion of the surface of the 1 x 4 mm samples. The ohmic contact was then annealed on a strip heater at 380^oC for one

minute in a flowing atmosphere of 5% H_2 in N_2. A copper wire was then attached to the ohmic contact with In solder.

The uncontacted portion of the $Ga_{1-x}Al_xAs$ was then etched in either a 15% HCl solution or in 0.5% Br in methanol for about 30 seconds. Etching of the ohmic contact was avoided by either covering it with black wax, or by dipping only the uncontacted portion of the sample below the surface of the etching solution. The best results were obtained with the HCl etch. Br-methanol often leaves a deposit on the sample surface, which results in poor Schottky barrier characteristics. After rinsing with DI water (500 kΩ-cm, from a Millipore Milli-Q DI system) and drying, the samples were immediately placed in an oil-free, ion pumped vacuum system. Gold dots about 130 microns in diameter were evaporated onto the samples through a stainless steel mask. The vacuum system pressure as measured at the ion pump was less than 10^{-6} Torr during the evaporation.

C. EXPERIMENTAL RESULTS

The mole fraction, x, of AlAs in the $Ga_{1-x}Al_xAs$ epitaxial layers was determined by electron microprobe analysis. Data reduction was performed using techniques developed by a number of workers, and refined by Bence and Albee for use on mineral samples [4,5].

In using the microprobe to find the concentration of one element

in a multicomponent system, one must account for effects such as x-ray absorption and florescence of the other elements in the system on the x-ray intensity for the element being analyzed. A linear, empirical relationship between the observed radiation intensity and the actual concentration of the element being studied can be used to approximate the effects of these corrections. For a binary system (alloy or compound), $\frac{1-K_A}{K_A} = \alpha_{AB} \frac{1-C_A}{C_A}$. This can be rearranged to give $\frac{C_A}{K_A} = \alpha_{AB} + (1-\alpha_{AB})C_A$, where K_A is the ratio of the x-ray intensity of A in the alloy to that of pure A, C_A is the weight fraction of A in the alloy, and α_{AB} is a specific correction constant for the measurement of A in the AB system. α_{AB} can be determined either experimentally or theoretically with fairly good results. This relationship can be generalized to more than two components for more complex alloys or compounds.

For this work, the electron beam energy was 15 keV. The data reduction was performed by Art Chodos of the Caltech Microprobe Laboratory using a computer program which makes corrections of the type mentioned above. It should be noted that the corrections for this system are rather large, as gallium and arsenic both have large absorption coefficients for the aluminum x-ray lines. This limits the accuracy of the measurement to a few percent for the samples, with large Al concentration. Estimates of the errors involved are indicated by the error bars in the figures.

Schottky barrier heights were measured using capacitance-
voltage, current-voltage, and photoresponse techniques. The results
of photoresponse and current-voltage measurements were in close
agreement with each other. Capacitance-voltage data were judged
less reliable than results of either the current-voltage or the
photoresponse measurements.

Current-voltage data for diodes for each composition measured
are shown in Fig. 1. The I-V characteristics follow the empirical
equation,

$$I = I_o(e^{qV/nkT}-1),$$

where n = 1.05, for several decades of current. Thermionic emission
theory can thus be used for determining the barrier heights. The
Schottky diodes on material with an AlAs mole fraction greater than
0.8 showed less ideal current-voltage characteristics than diodes
on $Ga_{1-x}Al_xAs$ with a smaller Al concentration. This was particularly
evident at high forward current levels.

These current voltage data were interpreted using density of
states effective mass data to compute the Richardson constant [6].
For the indirect band gap compositions, x > .43, the conduction band
minimum is anisotropic and consists of multiple minima in equivalent
symmetry directions. Use of the density of states effective mass
ignores this and could result in a small error (20 meV) in the bar-
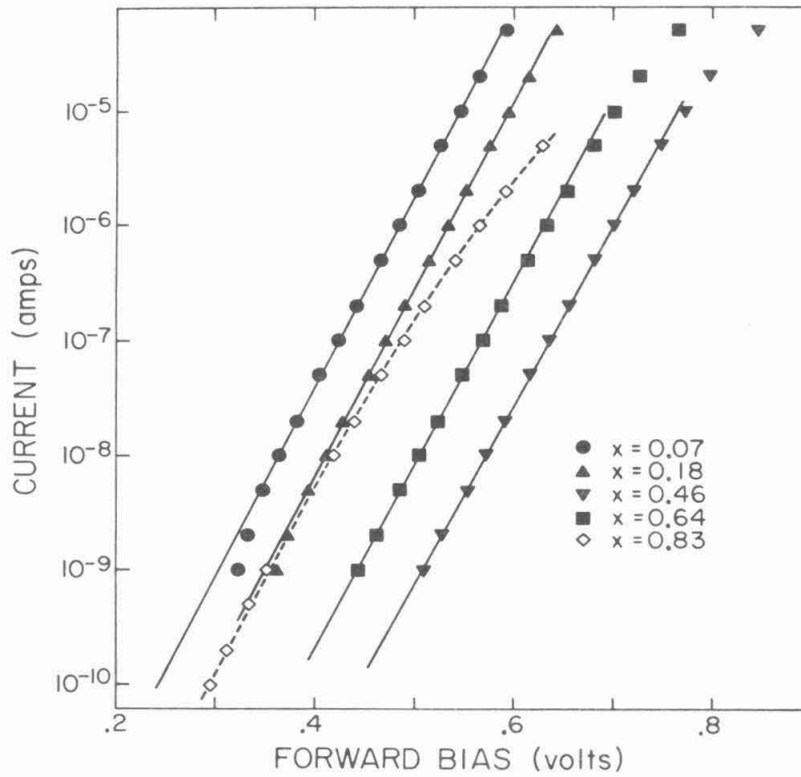
Fig. 1. Current-voltage characteristics of Au on n-Ga$_{1-x}$Al$_x$As Schottky barriers. The approximate area of the Au dots was 2×10^{-4}cm^2. The nonlinearity for high currents is due to ohmic contact and bulk resistance effects.

rier height determination. A correction was made to the barrier
height for the effect of image force lowering. The capacitance-
voltage determined carrier concentrations were used for that correc-
tion.

Photoresponse data, shown in Fig. 2,were plotted as the square
root of short circuit photocurrent per incident photon vs hν. A
straight line extrapolation to zero photocurrent gave the barrier
height, less the image force lowering correction. Less ideal
straight lines were obtained than with the current-voltage data,
but the barrier height values were in good agreement with those
obtained by I-V measurements.

Capacitance-voltage determined barrier heights were spread
over a range of several tenths of a volt on different gold dots on
the same sample. Within the limits of that uncertainty, agreement
with the current-voltage and photoresponse data was good for the
barriers on $Ga_{1-x}Al_xAs$ with x < 0.4. For larger Al concentrations,
the capacitance-voltage method gave a higher value for the Schottky
barrier height than current-voltage or photoresponse method by 0.1
to 0.3 eV. Crowell and Roberts [7] have shown, in a simple model,
that an interfacial oxide layer of 50 to 100 Å could account for a
higher capacitance-voltage barrier height of this magnitude.
Because the capacitance-voltage data had a much larger amount of
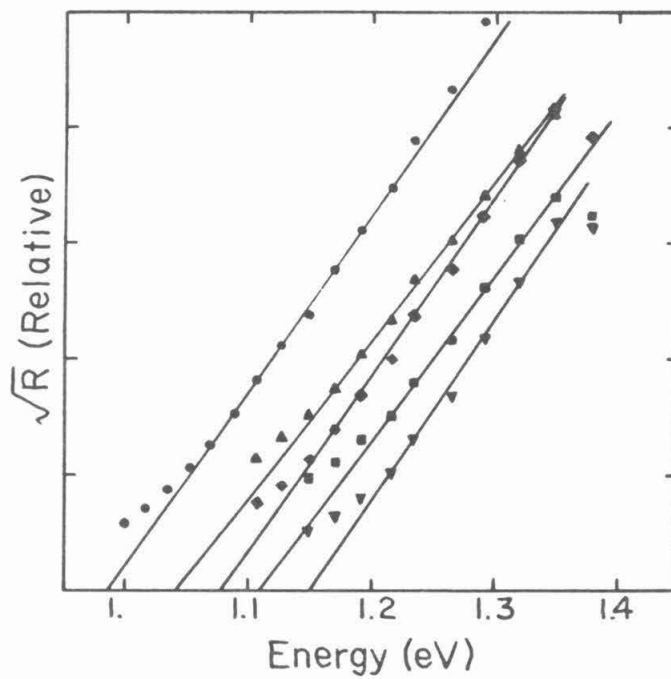
Fig. 2. Photoresponse chaacteristics of Au on n-Ga$_{1-x}$Al$_x$As Schottky barriers. χ = 0.07,   x = 0.18,   x = 0.46,   x = 0.64, x = 0.83.

scatter than photoresponse or current-voltage data, they were used primarily for determining carrier concentration.

A qualitative Auger profile was made of the $Au-Ga_{1-x}Al_xAs$ interface for samples with $x = 0.07$ and $x = 0.83$. Oxygen was present at the interface in both cases; however, there was several times as much oxygen at the $Au-Ga_{0.17}Al_{0.83}As$ interface as at the $Au-Ga_{0.93}Al_{.07}As$ interface, being detectable for ≈ 100 $\overset{o}{A}$ into the semiconductor.

Data for all three barrier height measurement techniques are summarized in Table I. For I-V and photoresponse the average values and estimated errors are given. For capacitance-voltage, the range of values observed for each composition are given.

Figure 3 shows results of barrier height measurements of Au on $Ga_{1-x}Al_xAs$ as a function of x. Also shown in the same figure is the $Ga_{1-x}Al_xAs$ band gap vs composition [6]. For small values of x, the barrier height on the n-type $Ga_{1-x}Al_xAs$ increases with increasing band gap. The slope of ϕ_n vs x is not, however, as steep as the slope of E_g vs x. For an AlAs mole fraction of ≥ 0.4, the barrier height decreases with increasing Al content, even though the band gap continues to increase. The barrier height on vacuum cleaved, pure n-AlAs [3] is also shown in the figure. It shows a larger value of ϕ_n than would be extrapolated from the chemically etched

TABLE I

	I-V	PHOTO	C-V
x = .07	0.93±.03	0.98±.03	0.97 - 1.1
x = .18	1.01±.03	1.08±.03	1.0 - 1.2
x = .46	1.18±.04	1.20±.03	1.1 - 1.5
x = .64	1.12±.04	1.17±.04	1.2 - 1.6
x = .83	1.03±.04	1.14±.04	1.1 - 1.3
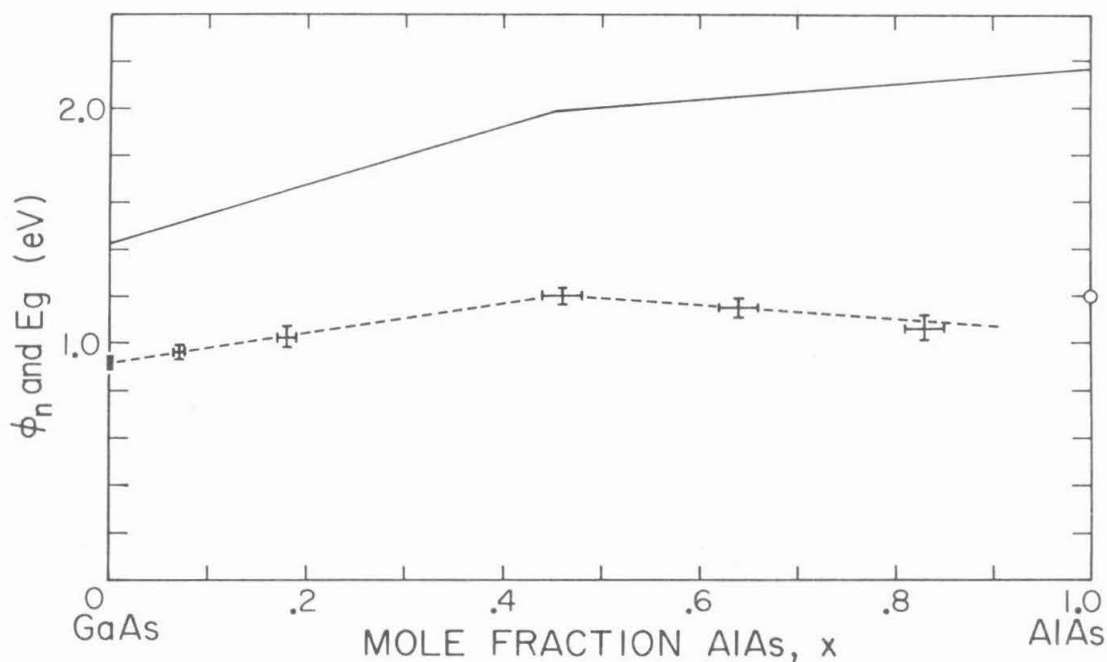
Fig. 3. Au on n-Ga$_{1-x}$Al$_x$As Schottky barrier height, ϕ_n, and band gap, E$_g$, as a function of x. ⊢⊣ indicates the values and estimated errors for the present work. ○ is the Au on vacuum-cleaved AlAs data of Mead, et al, and ▮ indicates accepted Au on GaAs Schottky barrier potentials.

$Ga_{1-x}Al_xAs$ data.

The deviation of the $Au-Ga_{1-x}Al_xAs$ Schottky barrier height from the common anion value is best observed in Fig. 4. Here, $(E_g - \phi_n)$ is plotted as a function of x. An alloy system, such as $Ga_xIn_{1-x}As$, which follows the common anion rule would be plotted as a horizontal line in this figure. The deviation of the Au on $n-Ga_{1-x}Al_xAs$ Schottky barrier energy from the common anion rule value is a linearly increasing function of Al concentration.

D. DISCUSSION

As pointed out in Chapter 1, various workers have recently reported the importance of interface chemical reactivity in determining Schottky barrier heights. It is well known that the AlAs surface is very reactive chemically, a fact which has made its growth difficult [8,9]. AlAs of poor crystalline quality is unstable even in air. The Au on $Ga_{1-x}Al_xAs$ samples in this work showed much greater oxidation for large AlAs mole fraction than for small AlAs content. This was directly evident in the Auger data, and was observed indirectly in the poorer quality of the I-V and C-V data for high Al concentrations. With a change in the chemical nature of the metal-semiconductor interface taking place as the AlAs mole fraction increases, it is not surprising that the "common anion" rule is not followed for Au on $Ga_{1-x}Al_xAs$.
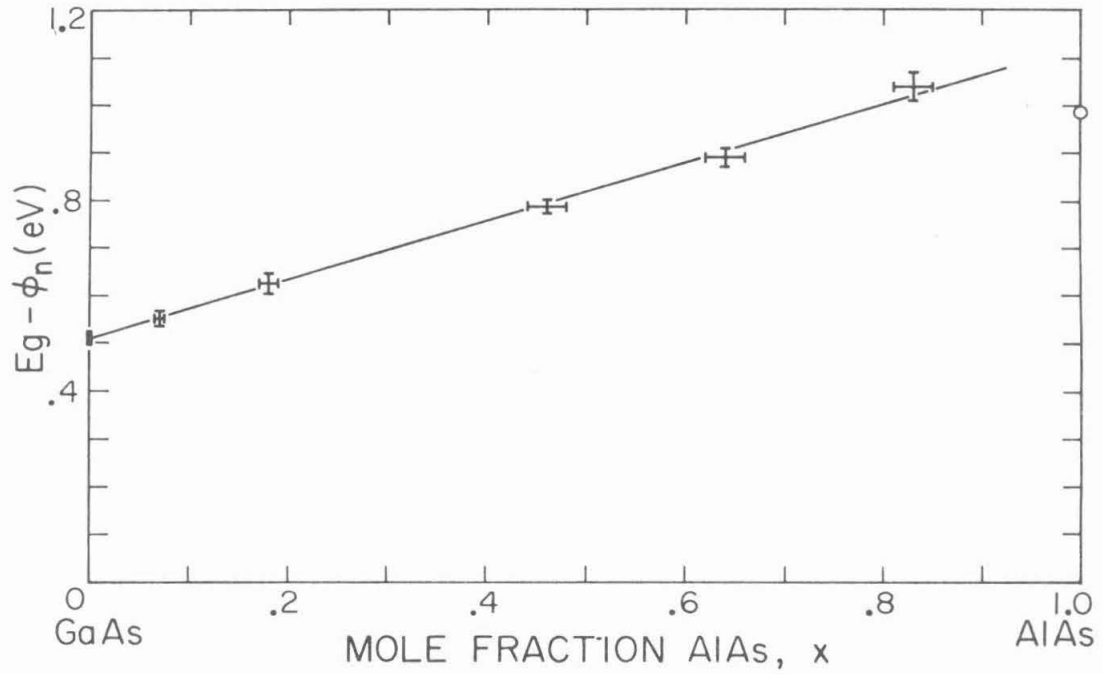
Fig. 4. Band gap minus Schottky barrier height, $(E_g - \phi_n)$, for Au on n-$Ga_{1-x}Al_xAs$ Schottky diodes plotted as a function of x. These data would lie on a horizontal line if the "common anion" rule were followed for this system.

Eliminating the air exposure of the $Ga_{1-x}Al_xAs$ surface, as by vacuum cleaving, reduces the deviation of the barrier height from the common anion rule value. This is seen in the vacuum-cleaved AlAs data plotted in Figs. 3 and 4. This vacuum cleaved preparation still gives a value for the Au/AlAs $(E_g - \phi_n)$ which deviates significantly from $(E_g - \phi_n)$ for GaAs and InAs. Modern improvements in AlAs quality and the use of UHV techniques - such as by in situ MBE AlAs growth followed by Schottky barrier formation and measurement - may reduce the deviation for pure AlAs further. It is doubtful, however, that oxidation is the sole reason for failure of the common anion rule, so that the deviation would probably not disappear completely no matter how carefully one did the experiments.

In summary, the Schottky barrier height of Au on $n-Ga_{1-x}Al_xAs$ has been measured as a function of x. The barrier height deviates, with increasing Al content, in a linear way from the value predicted by the common anion rule. This is attributed to the reactivity of the AlAs surface.

REFERENCES

1. K. Kajiyama, Y. Mizushima and S. Sakata, Appl. Phys. Lett. 23, 458 (1973).

2. T. F. Kuech, private discussion.

3. C. A. Mead, Solid State Electron. 9, 1023 (1966).

4. The Electron Microprobe, edited by T. D. McKinley, (Wiley, New York, 1966) pp 296-377, 378-389.

5. A. E. Bence and A. L. Albee, J. of Geology 76, 382-403 (1968).

6. H. C. Casey, Jr., J. Appl. Phys., 49, 3684, (1978).

7. C. R. Crowell and G. I. Roberts, J. Appl. Phys. 40, 3726 (1969).

8. A. G. Milnes and D. L. Feucht, Heterojunctions and Metal Semi-conductor Junctions (Academic, New York, 1972) p 144.

9. T. Tsukada, Appl. Phys. Lett. 28, 697 (1976).

APPENDIX I

SEMICONDUCTOR LATTICE PARAMETERS

Lattice parameters of the common group IV, III-V, and II-VI semiconductors are given in the table and chart on the following pages. These data were assembled and put into the form shown in the figure by J. O. McCaldin.

For convenience in determining heterostructure lattice mismatch, the values given for wurzite (hexagonal) structure materials are $\sqrt{2}\ a_o$. These values are indicated by an asterisk. Note that for ZnS, both zincblende (cubic) and wurzite values are given. Zinc blende is the room temperature phase; however, crystals grown at $\geq 1100^o C$ have the wurzite structure.

Substance	a_o (Å)	Ref.
Si	5.4309 (25°C)	1
Ge	5.43075 (300°K)	2
	5.658	3
AlP	5.462	4
GaP	5.451	4
InP	5.869	4
AlAs	5.662	4
GaAs	5.653	4
InAs	6.058	4
AlSb	6.135	4
GaSb	6.095	4
InSb	6.479	4
ZnS	5.409	4
	5.4093	5
	5.4095	2
	5.401 *	5
CdS	5.82 *	4
	5.8503 *	5
β-HgS	5.851	5
ZnSe	5.669	4
	5.6687	5
CdSe	6.07 *	4
	6.079 *	5
HgSe	6.084	5
ZnTe	6.104	4
	6.1037	5
CdTe	6.481	4
	6.481	5
HgTe	6.460	5

1. W. M. Yim and R. J. Paff, J. Appl. Phys. 45, 1456 (1974).

2. R. R. Reeber, Phys. Stat. Sol(a) 32, 321 (1975).

3. Monsanto Co. Some Properties of Semiconductors (1971).

4. L. M. Foster, J. Electrochem. Soc. 121, 1662 (1974).

5. W. L. Roth, in <u>Physics and Chemistry of II-VI Compounds</u> , ed. M. Aven and J. S. Prener, (Wiley, New York, 1967), Ch. 3.
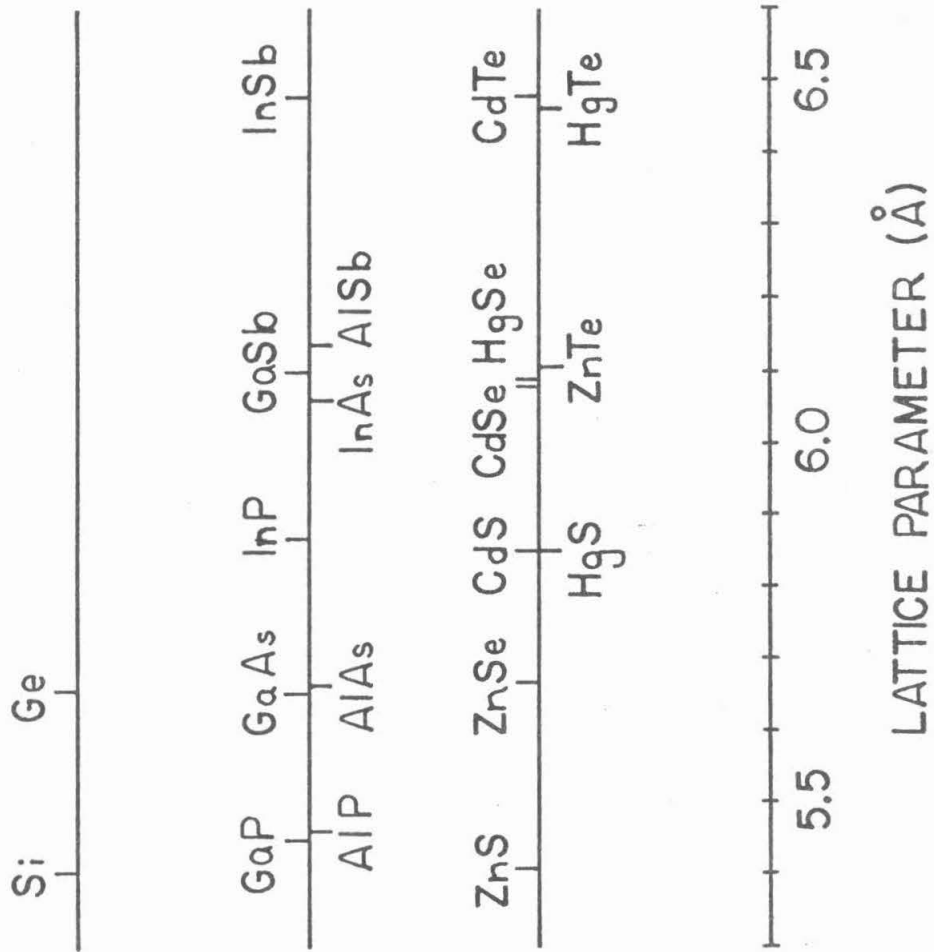
Fig. 1. Lattice parameters of common III-V and II-VI semiconductors.

APPENDIX II

SUBSTRATE PREPARATION

Evaporated HgSe contacts were in all cases deposited on substrates which were cleaved in air. Ohmic contacts were attached before cleaving so that the cleaved surface was not heated before deposition. A summary of the preparation techniques used for the various materials is given in Table II. Detailed descriptions of the more complicated processes follow. These recipes, although not developed by the author, are given here because they are not well known in the literature.

ZnS, as obtained from Eagle Pitcher was highly resistive, even with 100 ppm of Al dopant in the crystal. A heat treatment in liquid zinc is necessary to shift the stoichiometry of the ZnS sufficiently to increase the carrier concentration to a usable level. The following procedure is used:

1. Cut the ZnS into 60 mil thick wafers. The ZnS must be thin enough to allow diffusion to affect the entire bulk of the crystal in a reasonable length of time.

2. Place the ZnS crystals in a quartz basket; lower slowly into a quartz crucible containing molten zinc at $880^{o}C$. Argon must be flowing over the zinc to prevent

oxidation.

3. After 100 minutes in the zinc, remove the basket
and immediately dip in liquid indium at 500°C to dis-
solve the excess zinc wetting the crystal. Leave the
ZnS in the indium for only a few minutes.

4. Mechanically brush the indium from the ZnS while
it is still molten; the small amount of indium remaining
can be removed in HCl.

5. The molten zinc must be poured from the quartz
crucible before it solidifies, as it will crack the
quartz crucible, otherwise. This is not a problem
with the indium crucible.

Ohmic contacts to the ZnS can also be difficult, as the Schottky
barrier height for any metal on ZnS is fairly large, and the carrier
concentration in the ZnS cannot be made high enough to achieve an
ohmic contact by tunneling. A recipe which works is to wet a
fresh (scraped or cleaved) ZnS surface with a Hg-In amalgam, place
a piece of 41% Cd - 59% In on the Hg-In, wet the Cd-In with more
Hg-In, then heat to 450°C for one minute in an inert atmosphere
(N_2 or Ar).

ZnSe is treated in the same manner as the ZnS, except that a zinc temperature of 750°C is used. The same ohmic is also used, with even better results than for the ZnS.

TABLE II. SUBSTRATE PREPARATION

HgSe was used on the following

Material	Supplier	Dopant	Heat Treatment	Carrier conc. (cm^{-3})	Ohmic Contact
p-GaAs	Crystal Specialties	Zn		$1x10^{17}$	Au-Zn-Au 480°, 30 sec
p-GaP	Sumitomo	Zn		$2x10^{17}$	Au-Zn-Au 480°C, 30 sec
n-InP	RSRE	Sn		$3x10^{16}$	In solder
n-CdTe				$4x10^{17}$	In solder
n-ZnSe	Eagle Picher	100 ppm Al	750°C in Zn 100 min	$5x10^{17}$	Hg-Cd-In 450°C 1 min
n-CdSe	Eagle Picher	10 ppm In	750°C in Se vapor, 4 hrs evacuated capsule	variable	In solder
n-CdSe	Eagle Picher	un-doped		$3x10^{15}$	In solder
n-ZnS	Eagle Picher	100 ppm Al	880°C in Zn 100 min	$5x10^{16}$	Hg-Cd-In 450°C, 1 min
n-CdS	Eagle Picher	10 ppm In	none	$4.5x10^{17}$	In

ohmic information on other materials

Material	Supplier	Dopant	Heat Treatment	Carrier conc. (cm^{-3})	Ohmic Contact
n-GaAs					88% Au-12% Ge eutectic 380°C, 1 min
p-InP					Au-Zn-Au 480°C-30 sec-2 min

p-CdTe					Br-methOH etch, Au-Zn-Au 275°C,1-3 min
P-ZnTe	Eagle Picher	undoped	700°C in Te vapor in evac. capsule, 90 min	2×10^{16}	LiNO$_3$ solution 350°C, 1 min,cover with Au

APPENDIX III

CVD AND OXIDE REDUCTION THERMODYNAMICS

Computation of the equilibrium constant for CVD transport, reduction of metal oxides or any other chemical reaction is simply a matter of computing the free energy change for the reaction at the temperature of interest. For the case of H_2 transport CVD, the reaction is $H_2(g) + MX(c) \overset{\Delta G}{\underset{\rightleftarrows}{}} M(g) + H_2X(g)$, so that

$$\frac{[M][H_2X]}{[H_2][MX]} = e^{-\Delta G(T)/kT}. \; \Delta G(T) \text{ can be computed from known data at a}$$

given temperature by using either of the two sets of thermodynamic relations given below

$$\Delta H_T = \Delta H_{298,\text{prod.}} - \Delta H_{298,\text{react.}} + \int_{298}^{T} \Delta C_p \; dT$$

$$\Delta C_p - C_{p,\text{prod}} - C_{p,\text{react}}$$

$$\Delta S_T = S_{298,\text{prod}} - S_{298,\text{react.}} + \int_{298}^{T} \frac{\Delta C_p}{T} \; dT$$

$$\Delta G_T = \Delta H_T - T\Delta S_T$$

or directly

$$\Delta G_T = \Delta G_{298} - \int_{298}^{T} \Delta S_T{'} \; dT{'}$$

These formulae were implemented to compute ΔG for the H_2 transport CVD reactions and for the reduction of the oxides of a number of metal used in semiconductor work.

For Fig. (2), the reactions graphed are as follows:

A $Hg(g)+H_2S(g) \rightleftarrows HgS(c)+H_2(g)$

B $Hg(g) + H_2Se(g) \rightleftarrows HgSe(c)+H_2(g)$

C $Hg(g)+H_2Te(g) \rightleftarrows HgTe(c)+H_2(g)$

D $Cd(g)+H_2S(g) \rightleftarrows CdS(c)+H_2(g)$

E $Cd(g)+H_2Se(g) \rightleftarrows CdSe(c)+H_2(g)$

F $Zn(g)+H_2S(g) \rightleftarrows ZnS(c)+H_2(g)$

G $Zn(g)+H_2Se(g) \rightleftarrows ZnSe(c)+H_2(g)$

H $Cd(g)+H_2Te(g) \rightleftarrows CdTe(c)+H_2(g)$

I $Zn(g)+H_2Te \rightleftarrows ZnTe(c)+H_2(g)$
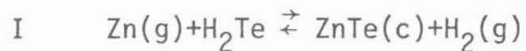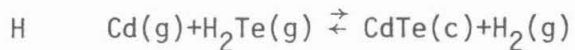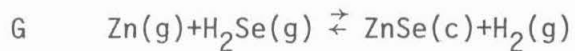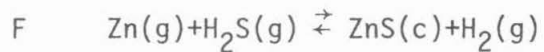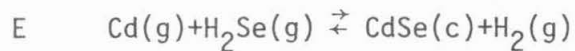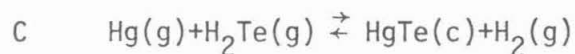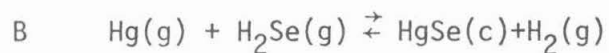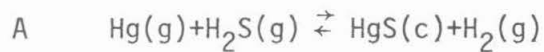
The calculations for this figure were made by L. Tutt.
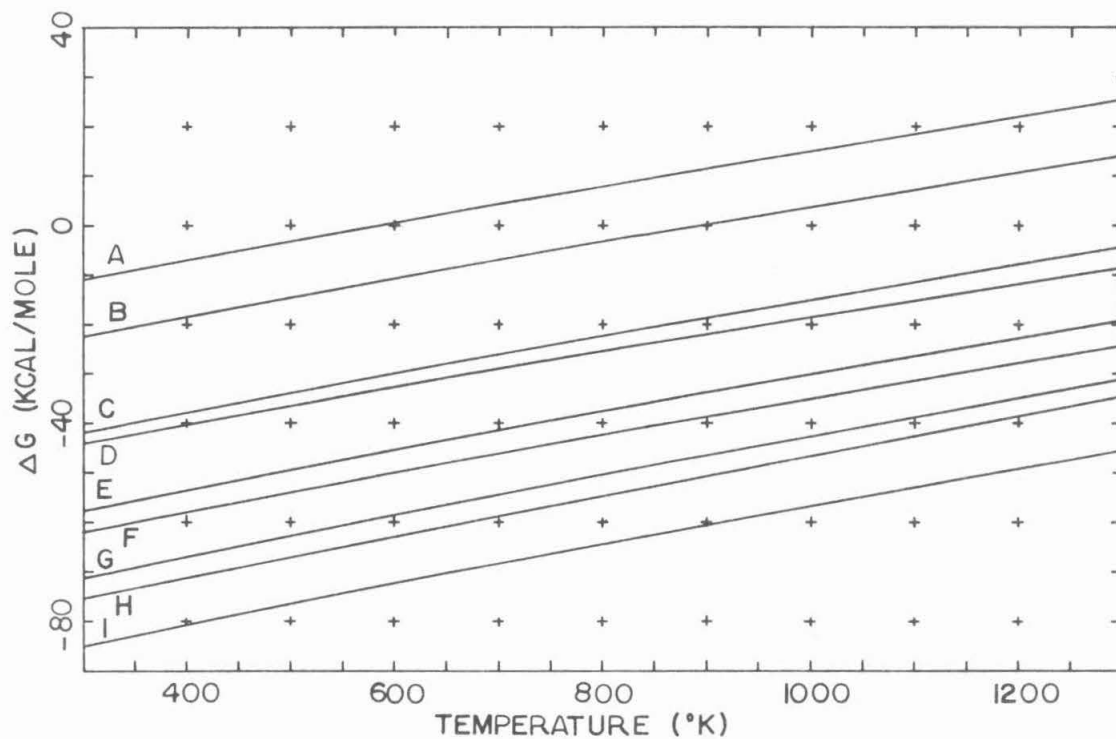
Fig. 2. Free energy change for H_2 transport CVD reactions listed in the text. Curve (A) is for HgS transport, (B) HgSe, (C) HgTe, (D) CdS, (E) CdSe, (F) ZnS, (G) ZnSe, (H) CdTe and (I) ZnTe.

In Figs. 3 and 4

ΔG and equilibrium $\dfrac{[H_2O]}{[H_2]}$ are shown for the following reactions.

Al: $Al_2O_3 + 3H_2 \rightarrow 2Al + 3H_2O$ $K = e^{-\Delta G/kT}$ $\dfrac{[H_2O]}{[H_2]} = K^{1/3}$

Cd: $CdO + H_2 \rightarrow Cd + H_2O$ $\dfrac{[H_2O]}{[H_2]} = K$

Ga: $Ga_2O_3 + 3H_2 \rightarrow 3H_2O + 2Ga$ $\dfrac{[H_2O]}{[H_2]} = K^{1/3}$

Ge: $GeO_2 + 2H_2 \rightarrow 2H_2O + Ge$ $\dfrac{[H_2O]}{[H_2]} = K^{1/2}$

In: $In_2O_3 + 3H_2 \rightarrow 3H_2O + 2In$ $\dfrac{[H_2O]}{[H_2]} = K^{1/3}$

Sn: $SnO_2 + 2H_2 \rightarrow 2H_2O + Sn$ $\dfrac{[H_2O]}{[H_2]} = K^{1/2}$

Si: $SiO_2 + 2H_2 \rightarrow Si + 2H_2O$ $\dfrac{[H_2O]}{[H_2]} = K^{1/2}$

Zn: $ZnO + H_2 \rightarrow H_2O + Zn$ $\dfrac{[H_2O]}{[H_2]} = K$
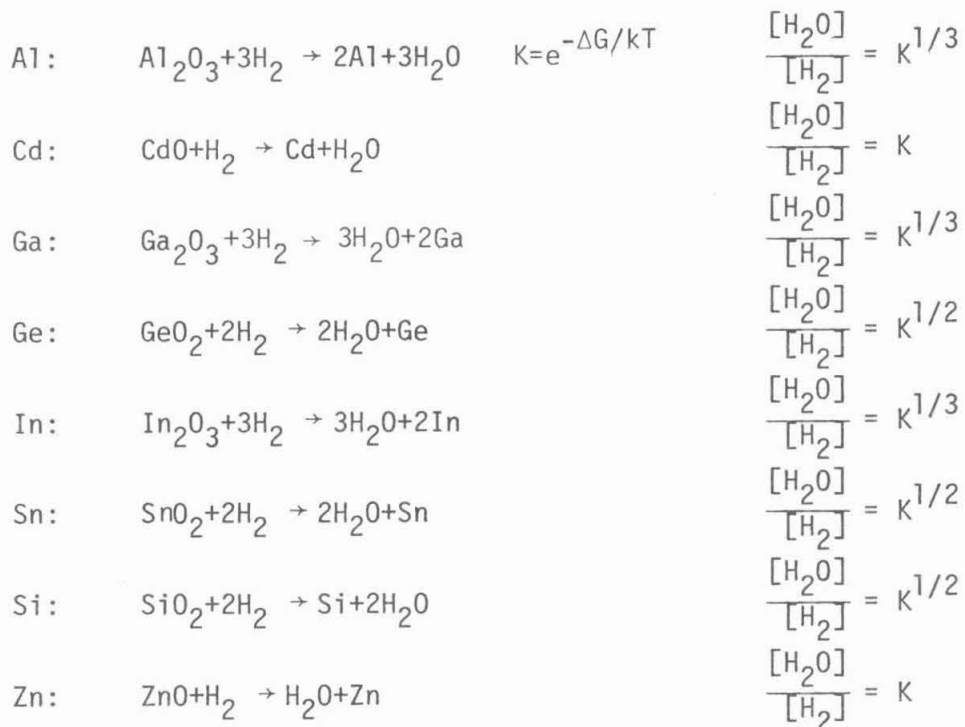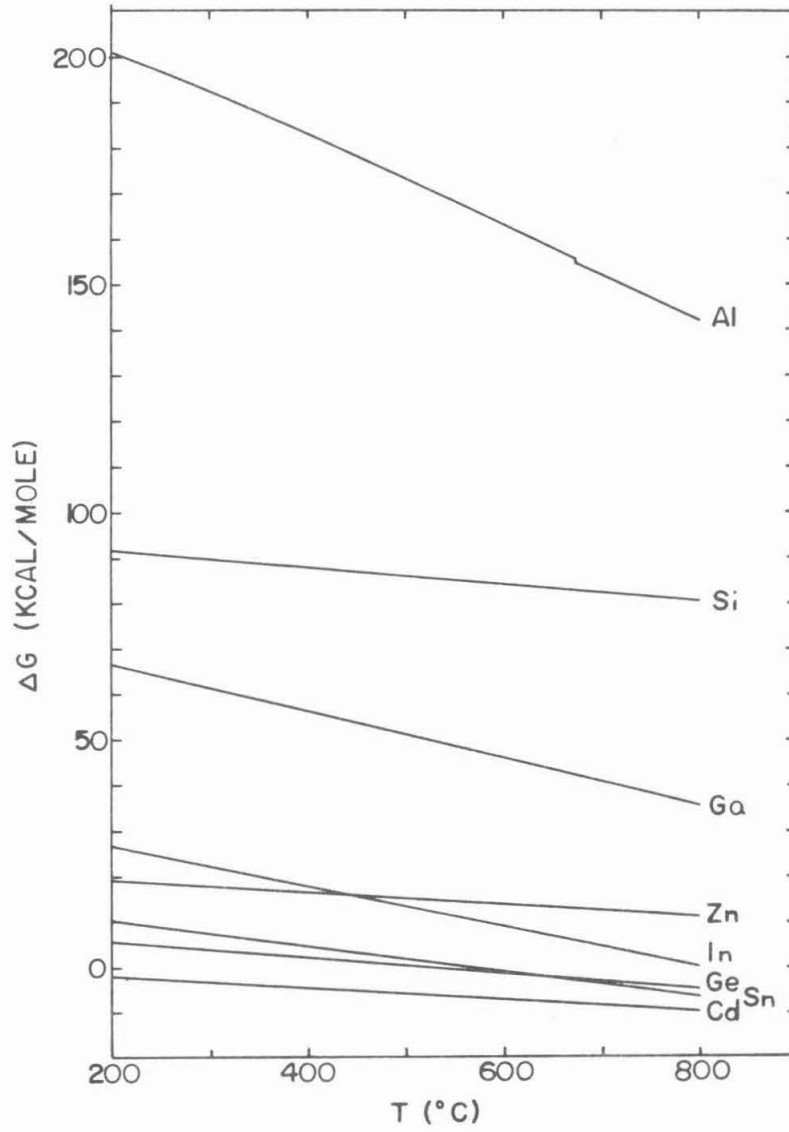
Fig. 3. Free energy change for oxidation/reduction of metals
shown. Reactions are given in the text.
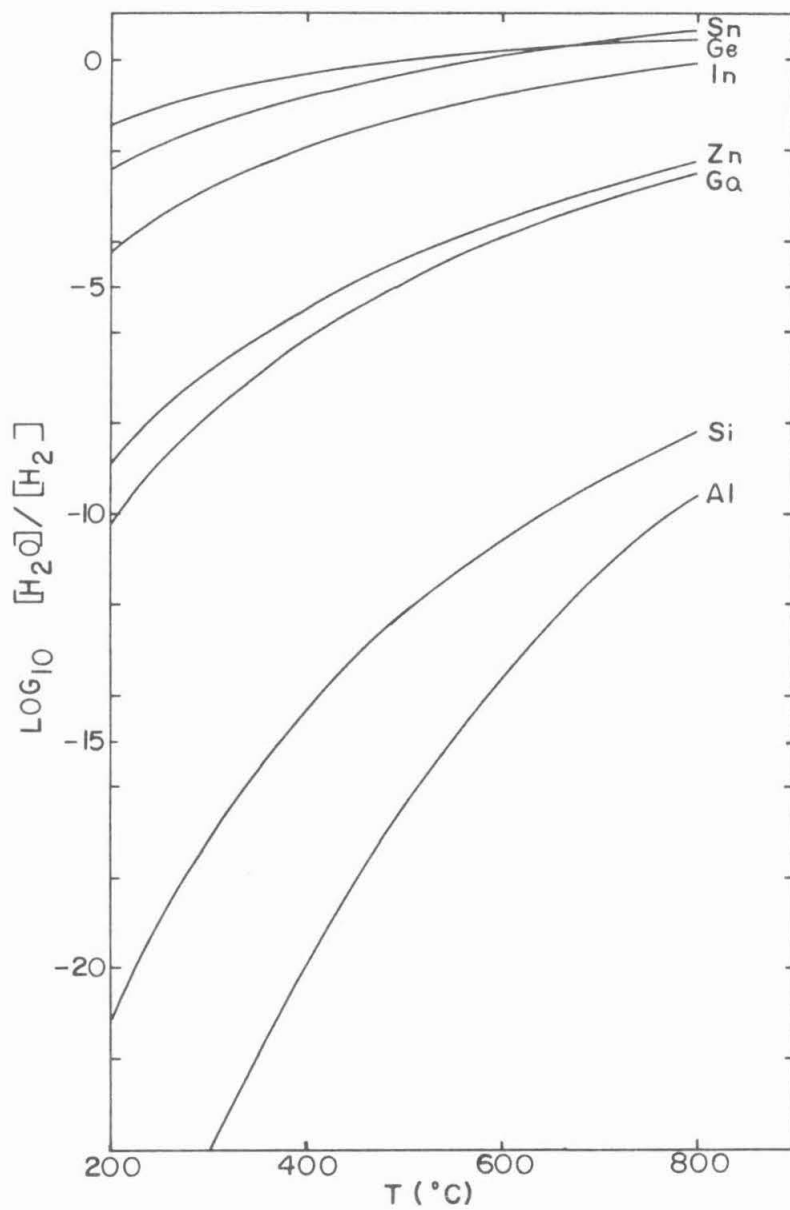
Fig. 4. Equilibrium water to hydrogen concentration ratios over the metals shown.